University of Münster
Institute of Landscape Ecology
Heisenbergstr. 2
D-48149, Münster

Turbulent fluxes of energy and CO$_2$ above a city:

A biannual eddy covariance study over Münster, Germany

Master thesis

Presented by Yang Zhao

Münster, August 2014

Supervisors:

Prof. Dr. Otto Klemm, University of Münster

Malte Julian Deventer, University of Münster

Contents

Abstract

In this work, a biannual dataset of carbon dioxide and other turbulent fluxes at a 65-meter-height tower in the center of a european city, Münster (NRW,Germany), was analyzed. The main purposes in this study are to outline the behaviors of CO_2 flux and to figure out the influences of factors on it and its yearly, seasonal and daily deviation. Additionally, the meteorological parameters from an automatic weather station, which is 3.1 km away from the tower, was also recorded for complement and comparison. The eddy covariance method had been used during the measurement and their qualities were checked in this study with the software 'Eddy Pro'. The whole measurement began in April, 2011 and ended in May, 2013.

Firstly, half-hourly means of carbon dioxide flux dividing in four seasons in each year are presented to find out the seasonal tendency. Combining with the meteorological parameter like the air temperatures in winters and springs in different years, it indicated that the warms season like spring and summer have a lower CO_2 flux than autumn and winter in a same year; the warm years had a lower flux than the cold ones. Secondly, through plotting a daily run of CO_2 flux, two peaks showed in the course because of the active traffic in the city. Additionally, energy fluxes are compared with the meteorological parameter and correlated to CO_2 flux: the vapor flux was related to the air temperature strongly and short-wave radiation had a positive correlation with the sun shine hours. Also, the vapor flux was related with CO_2 flux negatively at the day.

Another purpose to do the study is to examine the yearly net ecosystem exchange (NEE) in Münster. Because of the gaps in the recorded dataset it is necessary to precede a gap filling process. The NEE in Münster in 2012 accounted for 3.26 - 3.56 C kg m^{-2}. This value was compared with the ones in other cities.

At the end, the CO_2 flux was connected with the wind direction to point out the parts in the city with the stronger CO_2 flux. The results revealed, those parts, which have a stronger CO_2 flux, were extremely influenced by the human activities.

1 Introduction

## 1.1 Urban climate and turbulence concept

1.1.1 Urban climate

Processes determining and driving urban climatology are closely linked to the energy exchange between the urban surface and the atmosphere. The mutual dependencies of these processes are regularly studied at various spatial and temporal scales. In recent years the respective research in urban areas has increased because of the increasing importance of global climate change, worldwide urbanization, rapidly rising population, and progressing industrialization. These processes alter the physical surroundings and the aerodynamical characteristics of urbanized regions, which also lead to changes in the energy balance. Most of these alterations may be traced to causal factors such as air pollution, anthropogenic heat, surface waterproofing, thermal properties of the surface materials, and morphology of the surface and its specific three-dimensional geometry such as building spacing, height, orientation, vegetative layering, and the overall dimensions and geography of these elements. Other factors that must be considered are relief, closeness to water bodies, size of the city, population density, and land-use distributions. (Oke, 1988)

The urban boundary layer (UBL), which has the most direct interaction with the earth's surface, is the lowest layer of the troposphere over a city. It responds to the surface within a time scale of about a few hours or even less. The cardinality and the structure of the boundary layer change within a day. The urban surface is warmed up after sunrise. Thermal turbulence is produced in the boundary layer, which destroys the inversion, i.e. the nightly temperature gradient, and builds up a complete mixing within this layer. However, unlike the rural surface, the urban one does not form a strong stable layer after the sundown. It stores the heat from the daytime which is absorbed by the urban surface, and due to a lack of the turbulence it does not cool off as effectively as the rural boundary layer. The urban boundary layer is also called an urban canopy layer or, at night, an urban heat island.

The urban boundary layer can broadly be divided into two sublayers: the upper layer (Ekman-layer), which is near the free atmosphere and the ground layer (Prandtl-layer or Constant-Flux Layer). Additionally, the Constant-Flux Layer is

classified into 3 sub-layers as proposed originally by Oke (1976): the urban canopy layer, the urban turbulent wake layer or roughness layer, and the inertial layer. The whole Constant-Flux Layer normally exhibits the higher concentrations of materials and energy fluxes, which makes it well suited to examine the exchange between the earth and the atmosphere.
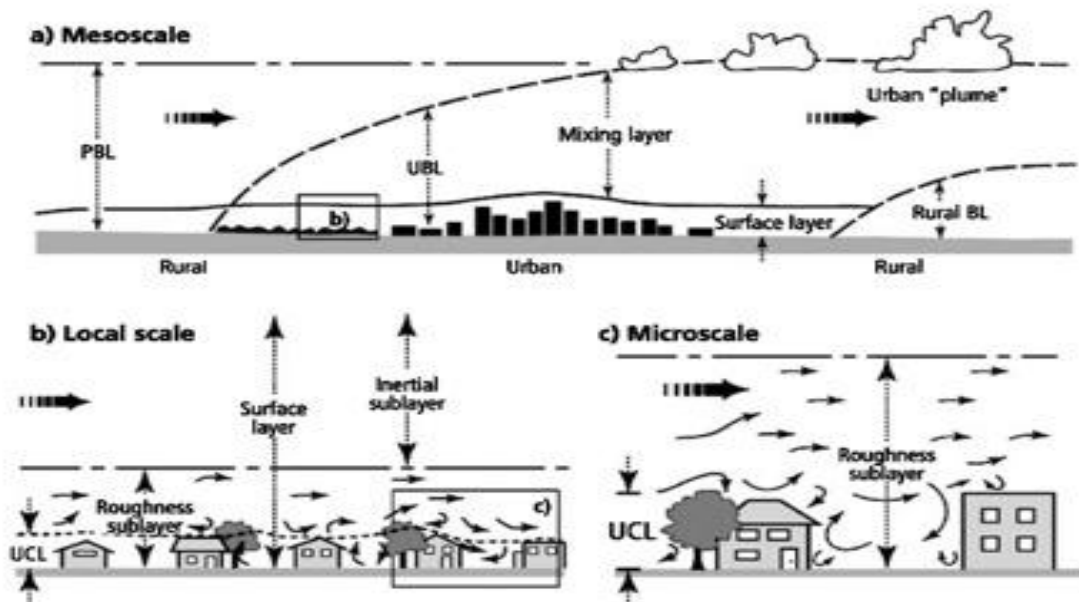
UBL: urban boundary layer; UCL: urban canopy layer

Fig. 1 The structure of the atmosphere layer: a) planetary boundary layer (PBL); b) Constant-Flux layer (from Fisher et al., 2005)

1.1.2 Turbulence concept

The urban surface is heated by the solar radiation which causes an ongoing production of thermal turbulence in the UBL. Turbulence is another state of a quasi random, short-termed and seemingly chaotic air packet motion in 3 dimensions varying in direction and speed. The fluctuation in temperature, wind speed, water vapor, heat and the substance concentration are all caused by atmospheric turbulence. It has four most obvious characteristics: high irregularity, diffusivity, rotationality and dissipation. Turbulences can be divided in two types: mechanical and thermal turbulence. The mechanical turbulence can be produced by two processes. One is wind shear during situations of high wind speed near the surface, and surface irregularity, which causes friction in the wind field. It is often greater than the effect of the wind shear. The length of the mechanical turbulence element is approximately 10 m and its temporal

scale is 10 s. On the other hand, the thermal turbulence shows a large spatial variabillity, it can extend from centimeters to hectometers and even kilometers. It lasts between 1 and 60 min. (Foken, 2003)

Since the turbulence is highly irregular, the fluctuations can only be described appropriately if they are divided into medium flows and deviations from that according to the concept of Reynolds.

$u=\bar{u}+u'$

$v=\bar{v}+v'$

$w=\bar{w}+w'$ *Eq. 1*

In order to present the three spatial wind components *u, v, w,* the respective averaged components, $\bar{u}, \bar{v}, \bar{w}$ in each 10 minute interval and their deviations *u', v', w'* at each instant of measurement must be calculated. This is the basis of the determination of vertical fluxes of, for example, momentum, heat, and water vapor, which are created by the turbulence. An exact measurement of the short-term fluctuation of wind, temperature and humidity is necessary.

The turbulence frequencies differ from 10^{-4} to 10 Hz (Foken 2003). For the results presented in this paper, the meteorological elements and fluxes are measured by a sonic anemometer with 10 Hz.

2 Study location

2.1 City of Münster
Münster is located in North Rhine-Westphalia (NRW), Germany, at latitude 51° 57' 36" North, longitude 7° 37' 34" East and 60 m above the sea level. This city ranks at the 62nd place among the 404 cities within Germany with a population of 291.754. Its area occupies 302.96 km². The residential areas make up a proportion of 23.19 % (Deutschland123.de). Therefore it has a relatively low overall population density of 979.0 per km^2 but still lies in the 10th place in NRW. (Tab.1)

Tab. 1 Top Ten of the largest cities in NRW (December 31, 2012)

Rank	City	Population	Area km^2	Density pro km^2
1	Köln	1 024 373	405,2	2 528,3
2	Düsseldorf	593 682	217,4	2 730,7
3	Dortmund	572 087	280,7	2 038,0
4	Essen	566 862	210,3	2 695,0
5	Duisburg	486 816	232,8	2 090,9
6	Bochum	362 213	145,7	2 486,7
7	Wuppertal	342 885	168,4	2 036,3
8	Bielefeld	328 314	258,8	1 268,6
9	Bonn	309 869	141,1	2 196,1
10	Münster	296 599	303,0	979,0

(it.nrw.de/statistik)

Münster has a marine west coast climate that is mild with no dry season, warm summers and moderate seasonality. According to the Holdridge life zones system of bioclimatic classification, Münster is close to the cool temperate moist forest biome. The annual average temperature is 9.5 degrees Celsius. Total annual precipitation averages 719 mm. Annual sunshine averages 1593 hours. (munster.climatemps)

Tab. 2 The annual average climate parameters in Münster, Germany

	Jan	Feb	Mar	Apr	May	Jun	Jul	Aug	Sep	Oct	Nov	Dec	Annual
Average Max Temperature °C (°F)	4 (39)	5 (41)	9 (48)	13 (55)	18 (64)	21 (70)	23 (73)	23 (73)	19 (66)	14 (57)	8 (46)	5 (41)	14 (56)
Average Temperature °C (°F)	2 (35)	2 (36)	5 (41)	9 (47)	13 (55)	16 (61)	18 (64)	18 (64)	15 (58)	10 (50)	6 (42)	3 (37)	10 (49)
Average Min Temperature °C (°F)	-1 (30)	-1 (30)	1 (34)	4 (39)	8 (46)	11 (52)	13 (55)	13 (55)	10 (50)	6 (43)	3 (37)	0 (32)	6 (42)
Average Precipitation mm (in)	68 (3)	53 (2)	45 (2)	53 (2)	49 (2)	57 (2)	84 (3)	70 (3)	62 (2)	56 (2)	63 (2)	59 (2)	719 (28)
Number of Wet Days (probability of rain on a day)	19 (61%)	16 (57%)	14 (45%)	16 (53%)	14 (45%)	13 (43%)	16 (52%)	16 (52%)	15 (50%)	17 (55%)	19 (63%)	18 (58%)	193 (53%)
Average Sunlight Hours/ Day	01:29	02:30	04:15	05:26	06:52	07:36	06:21	06:01	05:10	03:29	01:48	01:15	04:21
Average Daylight Hours & Minutes/ Day	08:19	09:50	11:47	13:51	15:39	16:37	16:11	14:36	12:35	10:32	08:44	07:49	12:00
Percentage of Sunny (Cloudy) Daylight Hours	18 (82)	26 (74)	37 (63)	40 (60)	45 (55)	46 (54)	40 (60)	42 (58)	42 (58)	34 (66)	21 (79)	17 (83)	36 (64)

(www.munster.climatemps.com)

Münster is largely characterized as a cultural landscape through the anthropological utilization. It occupies most of the area with 139.68km^2 (46.11%), while the residents take up 23.91%. The city center provides also parks, promenades, and other green belts, which take up 2.73%. (Deutschland123 AG, 2013). The residential zones differ from each other according to the ring-road system, which are mainly two- or three-story apartments or villas besides churches, public buildings or sights.
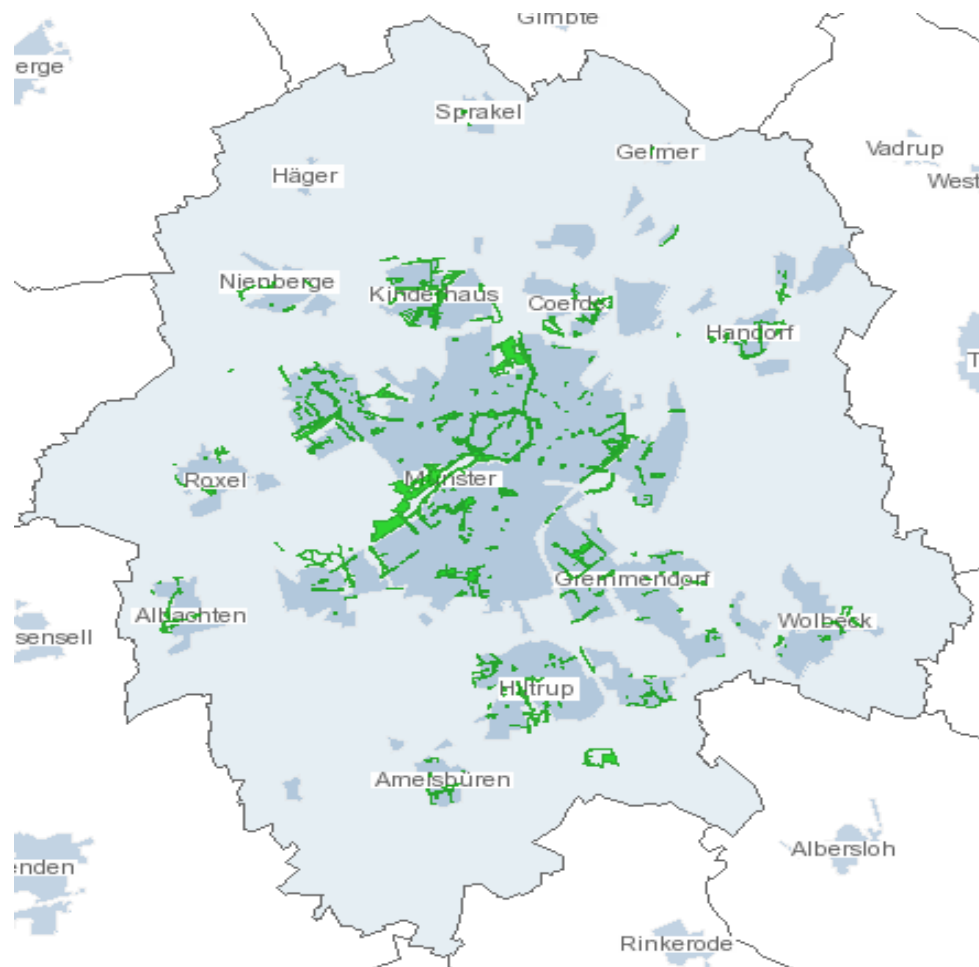

Fig. 2 The green space in the city center in Münster

(geo.stadt-muenster.de/stadtplanung)

In contrast to the predominantly agriculturally managed surrounding, the city itself exhibits major emissions from traffic, densely populated residential areas, power plants, small to medium size industrial plants (Gietl et al., 2008; Schmidt et al., 2008). It is also exposed to air pollution from long-range transport from various sources in Germany and neighboring countries

2.2 Measurement sites description

2.2.1 Radio Tower

The major measurement site takes place at a radio tower towards southeast of the city. The tower station lies downwind of the urban section because the south-westerly and westerly wind directions dominate.
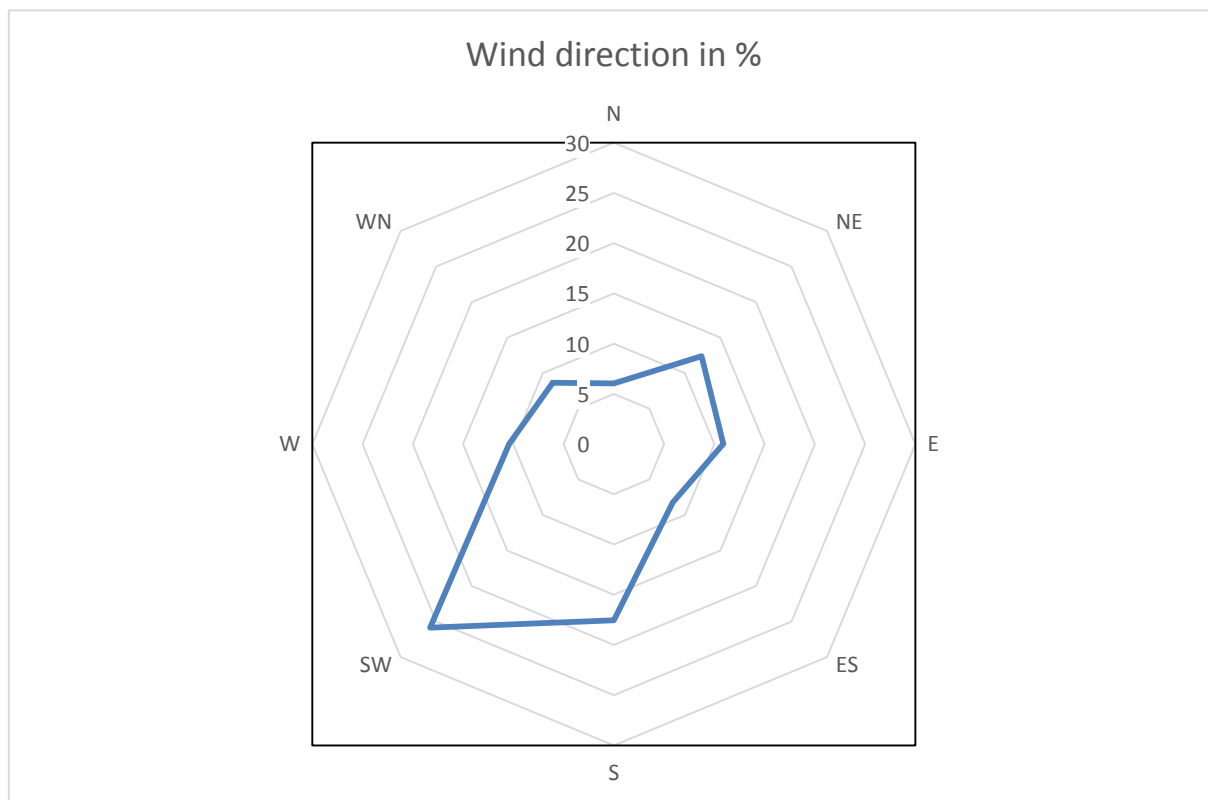

Fig. 3 Wind distribution in Münster from Jan. 2011 to Oct. 2013, observation at automatic weather station, Hüffergarten.

The experimental instrumentations were set up on top of the radio tower at a height of 65 m above ground level (a.g.l.) which was about 40 meter above the surrounding urban canopy. Based on earlier experience at this sampling location (Deventer, 2013) (Burda and Schmidt, 2012) the direction and the height of the setup was organized in a way that the flux footprint represents the urban region whenever the main wind direction is established. At the same time, it was outside the urban roughness layer.

2.2.2 Institute for Landscape Ecology, University of Münster

Another site of meteorological measurements is needed to fill the missing data resulting from measurement mistakes and the quality filtering. It is actually an automatic reference meteorological reference station, which is located at the roof of the Institute of the Landscape Ecology (ILÖK) of the University of Münster, 3.1 km to the West of the radio tower station, street address Robert-Koch-Str. 28, called "Hüffergarten". The sensors are set on a measurement pole at the roof of the building at a height of 4.4 m and total height 22 m above the ground. The atmospheric data series consists of air temperature, wind direction, horizontal wind speed, relative humidity, relative humidity, and shortwave radiation.
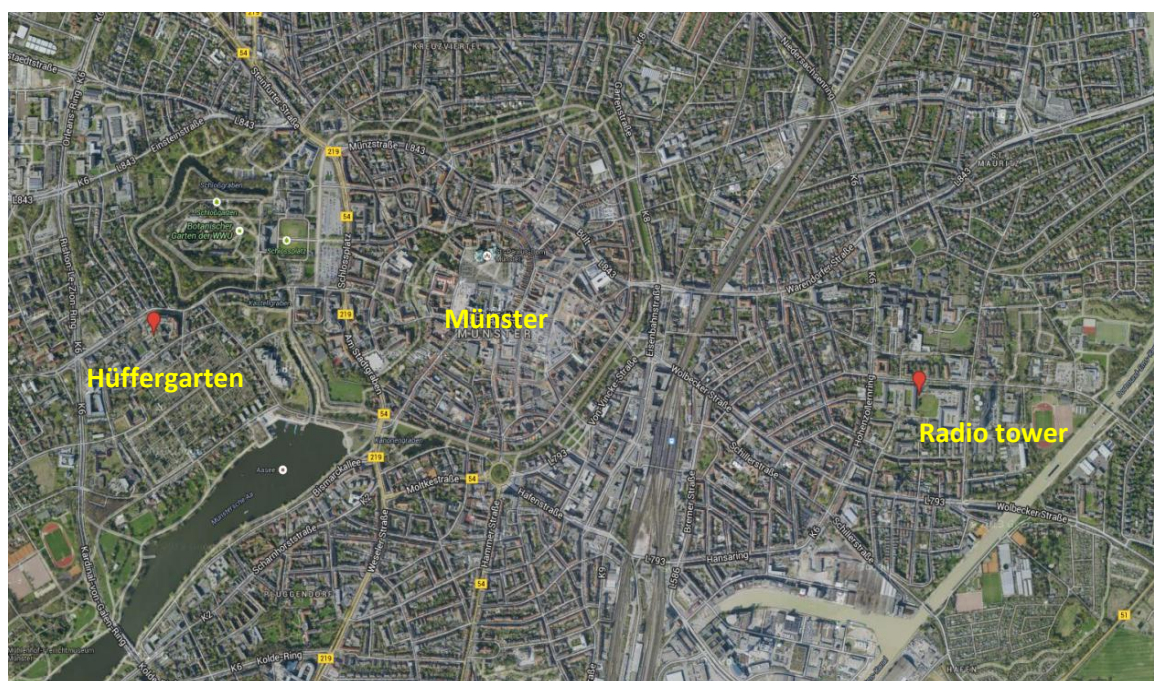

Fig. 4 Location of the two measurement sites in Münster (maps.google.de)

3 The experimental instrumentation

All data on the reference station are recorded with 10-minute-intervals. The water vapor concentration at the reference station was calculated from the relative air humidity and air temperature by using suitable algorithms (Buck 1981; Alduchov and Eskridge 1996). The air temperature and the relative humidity at the reference station in Hüffergarten were measured with a combined Pt-100 and a humidity sensor, which can not be influenced by rain. In contrast to the reference station, rain will exert influence on the measurements on the radio tower which was instrumented with the ultrasonic anemometer for the (virtual or "sonic") temperature, and with the LI-COR 7500

for the water vapor and CO_2 concentrations. The data of the atmospheric parameters which measured at the reference station are helpful to fill the gaps in the flux data series at the tower as caused by the rain events and instrumental outages.

The instrumentation on the radio tower included a sonic anemometer model R3-50 (Gill Instruments Limited, UK), an open path gas analyzer model LI-7500, and an enclosed gas analyzer model LI-7200 (LiCor Inc., Lincoln, Nebraska, USA).

3.1 R3-50 (Sonic anemometer)

The R3-50 3-axis anemometer is particularly suitable for determining fluxes using the eddy covariance technique. This precision ultrasonic anemometer will monitor wind speeds up to 45 m/s, with a fast data output rate of up to 50 Hz or 100 Hz (sets output to average 10 samples at 100 Hz for 10 Hz data). The three wind components u, v, w and SoS (sonic temperature) outputs are available. (Gill Company, 2014)

3.2 LI-7500 infrared gas analyzer

The LI-7500 is a high performance, non-dispersive, open path infrared CO_2/H_2O analyzer designed for use in eddy covariance flux measurement systems. It measures simultaneously the CO_2 and H_2O mixing ratios in the free atmosphere. It is suitable for a high speed measurement and internal 150 Hz measurements are digitally filtered to provide a true 5, 10, or 20 Hz bandwidth. Exposures to rain or snow do not damage or shift the calibration. (Licor.com)

3.3 LI-7200 infrared gas analyzer

The LI-7200 is a high performance, non-dispersive, however, enclosed path infrared CO_2/H_2O analyzer designed for use in eddy covariance flux measurement systems. Similar to the LI-7500 it is also suitable for a high speed measurement and internal 150 Hz measurements are digitally filtered to provide a true 5, 10, or 20 Hz bandwidth. The LI-7200 is based on the design of LI-7500A. It uses an enclosed path sampling cell. Unlike other closed path instruments, the LI-7200 is designed to be used with a short intake tube, because the analyzer is weatherproof and can be mounted outside on a tower. The design of the LI-7200, along with its low power requirements, allows it to be used in a variety of applications, including Eddy Covariance. (Licor.com)

4 Methods

4.1 Operation Theory of Infrared Gas Analyzer

In short, the operation theory relates to the absorption of infrared light by the gas of interest in the air. Different molecules in the atmosphere can absorb different frequencies of light, and according to the scaling law of Jaimeson et. al. (1963), they show the effect of infrared absorption according to their respective partial pressures.

4.2 Operation Theory of Ultrasonic Anemometer

An ultrasonic anemometer has normally three pairs of sensors on three different axes. Each sensor can transmit and receive ultrasonic signals. The speed of sound is thus recorded in the three kartesian axes.

Sonic anemometers operate by measuring the time taken for a pulse of sound to travel between a pair of transducers. This time depends on the distance between the transducers, the speed of sound, and the air speed along the axis of the transducers. (Gill Instruments Limited, 2014).

A wind component in direction of an axis leads to an increase of the travel speed of sound waves, noted as a 'forward-wind', while at the same time, a wind component against the wind direction leads a reduction, a 'back-wind'. The wind speed and its direction can be calculated from the time interval on each sensor as follows:

$$t_{forward} = \left(\frac{d}{c+v}\right);$$

$$t_{back} = \left(\frac{d}{c-v}\right) \qquad \qquad \textit{Eq. 2}$$

where $t_{forward}$ and t_{back} are the run times of the sound forward and back, d is the distance between the sensors, c is the speed of sound, and v is the air speed along the axis.

Since each sensor alternates as transmitter and receiver in both forward and backward directions, the air speed and sound speed can be described as follows:

$$v=0.5d \left(\frac{1}{t_{forward}} - \frac{1}{t_{back}}\right);$$

$$c=0.5d \left(\frac{1}{t_{forward}} - \frac{1}{t_{back}}\right) \hspace{3cm} \textbf{\textit{Eq.3}}$$

After measuring the three-dimensional speed components and transforming them in a polar coordination system, the wind speed and its direction is obtained by use of the trigonometric function arc tan:

$$|v| = \sqrt{v_x{}^2 + v_y{}^2} \hspace{3cm} \textit{Eq. 4}$$

In a still and dry air, the speed of sound depends on:

$$c = \sqrt{\kappa \bullet R_d \bullet T} \hspace{3cm} \textit{Eq. 5}$$

The virtual temperature of a moist air parcel refers the temperature at which a theoretical dry air parcel would have a total pressure and density equal to the moist parcel of air (Wikipedia). For moist air, a density correction by using the virtual temperature T_v can be performed:

$$c = \sqrt{\kappa \bullet R_d \bullet T_v} \hspace{3cm} \textit{Eq. 6}$$

where к is adiabatic exponent = 1.4, R_d is mass-specific gas constant in dry air = 287.04 J kg^{-1} K^{-1}. Hence, the virtual temperature can be expressed as:

$$T_v = \frac{c^2}{\kappa \bullet R_d} = \frac{c^2}{402.314} \ (K) \hspace{3cm} \textit{Eq. 7}$$

In this context, the virtual temperature is also taken as the sonic temperature. However, it is worthy to notice, the virtual temperature differs slightly from the real temperature.

In conclusion, the horizontal wind speed and direction, the vertical wind component, and the virtual temperature can be recorded with a frequency of 10 Hz by using an ultrasonic anemometer. From the recorded parameters, other relevant parameters like turbulent momentum flux, friction velocity and stability can be derived. Parameters that are important for data quality control such as integral characteristics of turbulence and stationarity of data subsets can be derived from the time series. All measurements are represented in 30-minute intervals.

4.3 Eddy Covariance

The eddy covariance method is widely used in micrometeorology, ecology and other environmental science fields. A typical eddy covariance system consists of an infrared gas analyzer and an ultra-sonic anemometer. This system focuses on the measurement and determination of the vertical turbulent fluxes in the atmospheric boundary layer. It is often used to estimate the heat, water vapor, carbon dioxide or methane fluxes.

The fundamental concepts of the eddy covariance method in turbulent fluxes measurements were originally suggested by Swinbank and Obukhov (1951). Fast response sensors are needed during the measurement with the eddy covariance to record the whole spectrum of turbulent fluctuations. The measurement of the air temperature, wind speed, wind direction, humidity and other gas is typically realized at 10 Hz or 20 Hz. The fundamental equation of the eddy covariance method is actually a simplified version of the equation proposed by Navier-Stokes for momentum, using the Reynolds' postulate. According to the Reynolds' decomposition of time series, a certain quantity X can be described as the sum of its average $\bar{X}$ and the deviation from this average X' (Mauder and Foken, 2011) , so the equation can be expressed as:

$$X = \bar{X} + X'$$ *Eq. 8*

This equation can be extended on the horizontal-, lateral-, vertical winds:

$$u = \bar{u} + u'; v = \bar{v} + v'; w = \bar{w} + w',$$ *Eq. 9*

The eddy covariance method can be only applied with the assumption of stationary and homogeneity. A flux F of a scalar s can be formulated as:

$$F = \overline{\rho \cdot s \cdot w}$$ *Eq. 10*

The essence of this method is that the vertical flux can be presented as a covariance of the vertical velocity and concentration of the entity of interest. That means that when the turbulent flux of a scalar quantity s and the vertical wind component w would be measured at the same point in time and space, this turbulent flux can be calculated by determining its covariance with the vertical wind component.

By using the Reynolds decomposition, Eq. 10 can be broken into means and deviation:

$$F = \overline{(\bar{\rho} + \rho')(\bar{w} + w')(\bar{s} + s')} \,, \qquad\qquad \textbf{\textit{Eq. 11}}$$

Also as:

$$F = \overline{\bar{\rho} \cdot \bar{w} \cdot \bar{s}} + \overline{\bar{\rho} \cdot \bar{w} \cdot s'} + \overline{\bar{\rho} \cdot w' \cdot \bar{s}} + \overline{\bar{\rho} \cdot w' \cdot s'} + \overline{\rho' \cdot \bar{w} \cdot \bar{s}} + \overline{\rho' \cdot \bar{w} \cdot s'} + \overline{\rho' \cdot w' \cdot \bar{s}} + \overline{\rho' \cdot w' \cdot s'}$$

$$\textbf{\textit{Eq. 12}}$$

The averaged deviation from the average is zero and as an assumption the density fluctuation can be neglected. Thus, the equation is simplified as follows:

$$F = \overline{\rho \cdot s' \cdot w'} \qquad\qquad \textbf{\textit{Eq. 13}}$$

Similarly, a momentum flux can be also determined with the same method. A friction velocity is depended on the shear stress on a surface. It can be expressed,

$$\tau = -\overline{w' \cdot u'}$$

$$u^* = \sqrt{\frac{\tau}{\rho}} = \sqrt{-\overline{w' \cdot u'}} \qquad\qquad \textbf{\textit{Eq.14}}$$

The friction velocity u* is a measure for the turbulent momentum exchange.

The Obukhov-Length is used to describe the effects of buoyancy on turbulent flows. It is a measure of stability. At a strong buoyancy force the layering is labile, contrarily, if at a weak or even negative buoyancy force, the layering would be neutral or stabile.

Obukhov-Length: $L = -\dfrac{u^{*3}}{k\frac{g}{T}\cdot\frac{Q_H}{\rho\cdot c_p}}$ $\qquad\qquad$ **_Eq. 15_**

Furthermore, a stability parameter $\xi = \dfrac{z}{L}$ is usually used to judge the stability.

All the turbulent fluxes in this study are recorded with 30 minutes, because a shorter time can result in a diminished representation of the long term flux in the data series. On the other hand, a time integration period longer than 30

minutes will lead to the risk that the atmospheric conditions are not stationary any more.

4.4 Data arrangement

A measurement can be never perfect due to non-perfect fulfillment of the mathematical assumptions, due to unsuitable meteorological condition, instrumental errors and more. Thus, it is necessary to filter the erroneous and low-quality data and to apply statistical corrections before further data analysis.

4.4.1 Arrangement with 'Matlab'

The raw files were arranged with 2 software packages, respectively, 'Matlab' and 'Eddy pro', so that before the calculation and analyses several correction processes could be completed.

It is important to notice the times when the day light saving time began and ended. The clock should be put back 1 hour between Sunday, 30th October 2011, 02:00:00 and Sunday, 25th March 2012, 02:00:00, and similarly between 28th October 2012, 02:00:00 and Sunday, 31th March 2013, 02:00:00.

The whole measurement period for this study lasted about 25 months, from 7th April, 2011 till 22th Mai, 2013. During this period, the infrared gas analyzers were exchanged several times, and the different instruments outputted different units. Cautiously, before further advanced corrections with 'Eddy Pro' were processed, the units were carefully checked. For example, the units of the CO_2 and H_2O concentrations were outputted as parts per million and parts per billion from the Li7200, while the Li7500 operated with molar concentrations. Additionally, different temperature and pressures were recorded through the gas analyzer. Table 3 shows further details.

Tab. 3 Units of CO_2 and H_2O, temperatures and pressures outputted with 2 different gas analyzers, and the time periods during which the analyzers were employed.

Instruments	
Li7200	**Li7500**
	20110407-20120312
20120403-20130212	
	20130212-20130221
20130221-20130514	
	20130514-20130522
Units of CO_2 and H_2O	
CO_2: ppm (parts per million)	CO_2: μmol/m^3
H_2O: ppt (parts per thousand)	H_2O: mmol/m^3
Temperatures and Pressures	
Average cell temperature	Ambient temperature
Cell pressure	Ambient pressure

4.4.1.1 Active gain control (AGC) and measuring errors

Firstly, the raw data would be handled with the software package 'Matlab' and checked if the active gain control (AGC) of the LI 7200 or LI 7500 exceeded the threshold of 70. Eventually, 25.3 % of the data were excluded from further analysis because of a large AGC value. Furthermore, 0.1 % of the remaining data were obviously erroneous ('-9999') and were thus deleted as well.

Secondly, due to electronic noise or other physical reasons, the data sets contain spikes in the high frequency range. These spikes were removed and replaced with a mean values. However, while removing spikes, it is required to look at the momentary data periodically to make sure that the applied removal criteria are suitable for the respective conditions (ECbook, 2013, Licor). Too strict criteria would cause the removal of too much data. In this study, it was decided to set absolute limits for the fluxes. For example, the fluxes of carbon dioxide, water vapor have limits of ± 100 μmol s^{-1} m^{-2} and ± 100 mmol s^{-1} m^{-2}, respectively. The sensible heat flux limit was ± 500 W m^{-2}, and for the latent heat flux, the limit is ±100 W·m^{-2}. All data were erased if they exceeded their respective limits. Another de-spiking criterion was to set a maximum allowed limit for standard deviations (SD) within single data sets. A criteria period was set to be the same season in the same year. Firstly, limits of ±3.5 SD were applied so that all data outside this range were removed from the data sets. If there were still some obvious spikes, a stricter criterion was set (Tab.4).

The seasons were, according to the meteorological convention, analyzed separately. Spring begins in March and ends at the last day in May; summer begins in June and lasts until the end of August; autumn lasts in the following 3 months until winter begins on the 1st December. The spike analyses and removals were performed within one-season data subsets. The respective criteria and the proportion of spikes of each parameter are shown in table 4.

Tab. 4 De-spiking criteria for each flux in a given period

(in standard deviation)		CO_2	H_2O	Tau	Sensible Heat	Latent Heat	Shear Velocity	Wind Speed	Vertical wind direction
Spring	2011	3.5	3.5	3.5	3.5	3.5	3.5	3.0	3.5
	2012	3.5	3.5	3.5	3.5	3.5	3.5	3.0	3.5
	2013	3.5	3.5	3.5	3.5	3.5	3.5	3.0	2.0
Summer	2011	3.5	2.0	3.5	3.5	3.5	3.5	3.0	3.5
	2012	3.5	3.5	3.5	3.5	3.5	3.5	3.0	3.5
Autumn	2011	2.0	3.5	3.5	3.5	3.5	3.5	3.0	2.0
	2012	3.5	3.5	3.5	3.5	3.5	3.5	3.0	3.5
Winter	2011	3.5	3.5	3.5	3.0	3.5	3.5	3.0	3.5
	2012	3.5	2.0	3.5	3.5	3.5	3.5	3.0	3.5
Proportion of spikes		0.71%	0.38%	0.44%	0.10%	0.23%	0.70%	0.72%	0.95%

4.4.2 Arrangement with 'Eddy Pro'

The remaining data was imported into the 'Eddy Pro' package and further statistically analyzed.

4.4.2.1 Coordinate rotation:

Because of an imperfectly settled sonic anemometer, its *w*-axis is not oriented exactly perpendicular to the mean flow. A double rotation for 30 minutes intervals (Kaimal and Finnigan, 1994) was used to rotate the coordinates so that the mean *w* equals to zero. This process can be done in several steps. First step: to rotate to make $\bar{v}$=0; $\tan \gamma = \frac{\overline{v_m}}{u_m}$. Second step: rotate to make $\bar{w}$=0; $\tan \alpha = \frac{\overline{w_m}}{u_m}$. Third step: rotate $\bar{w} \cdot \bar{v}$=0, however, it is rarely used because it can create unrealistic values (Aubinet, *et al*, 2003).
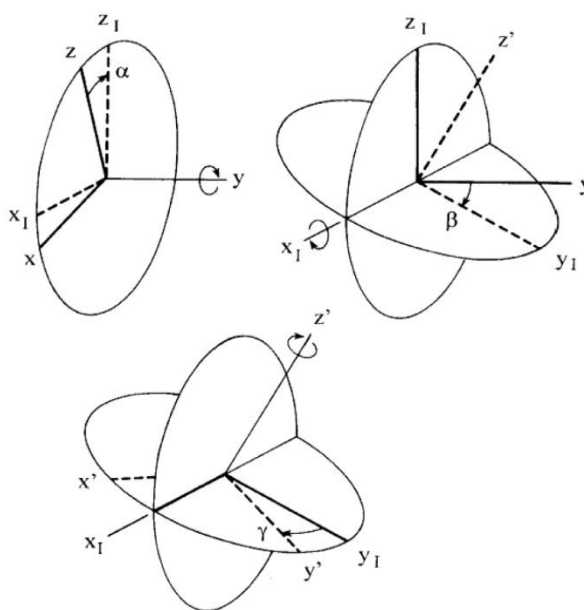
Fig. 5 Definition of rotation angles after Wilezak et al. (2001)

4.4.2.2 Correcting for time delay

The correction for time delay is applied to compensate the delay in signal acquisition from different instruments, i.e. the time series of sonic anemometer and gas analyzer.

This is especially important when using a closed-path instrument with a long intake tube, as air sampled by the sonic anemometer may arrive at the closed cell many seconds later than the *w*-signal. For enclosed-path and open-path analyzers as employed here, the time delay is much smaller, but it also should be compensated for to avoid flux losses. (EC book, 2013. Licor)

If the time delay was not corrected the fluctuations in w' might not match the ones of the gas concentration, and the resulting fluxes can be underestimated, even reach zero values.

Time delay is usually corrected in one of two ways, or in combination:

1. theoretically, via flow rate, tube diameter, etc.

2. empirically, by running circular correlation, shifting the delay scan-by-scan until maximum correlation (flux) is found.(EC book, 2013. Licor)

A combination of theoretical and empirical methods was used to correct the time delays in this study. It worked well and yielded reliable values for all gas analyzers.

4.4.2.3 De-trending (linear de-trending):

One of the conditions for the applicability of the eddy covariance method is the stationarity of data sets. No trend should be presented in the data. To ensure this and to differentiate the turbulent transport, measured with the eddy-covariance-method, from slow, large-scale movements, a de-trending process has to be used.

During de-trending, mean values are subtracted from instantaneous values before computation of the flux. This requires the computation of the mean for a given time series. There are three main, traditional ways to look at it, along with three respective techniques: block averaging, linear de-trending, and non-linear de-trending. (EC book, 2013.LiCor). Linear de-trending was selected to avoid low frequency losses (Gash & Gulf, 1996). The algorithm consists of

calculating a linear regression between the time values and the specific data values in the first step. Then the linear trend represented by the slope of the regression line is subtracted from the time series, so that the new mean matches the former one. (Kolle & Rebmann, 2007)

4.4.2.4 Data quality control (Foken classification)

The data quality control is based on two tests: steady-state test and integral turbulence characteristics test. The steady-state test according to Foken and Wichura (1996) is based on developments of Russian scientists (Gurjanov et.al. 1984) and compares the statistical parameters determined for the averaging period and for short intervals within this period. For instance, the time series for the determination of the covariance of the measured signals w (vertical wind) and x (horizontal wind component or scalar) of 30 minutes duration will be divided into 6 intervals of 5 minutes. This value will be compared with the covariance determined for the whole interval. A time series is considered to be steady state if the difference between both covariances is lower 30 %. (Documentation and introduction manual of the EC software package TK3, Thomas Foken).

This value is found by long experiences but is in a good agreement with other test parameters also of other authors (Foken and Wichura 1996)

To test the development of turbulent conditions, the so-called flux-variance similarity is a good measure. This similarity means that the ratio of the standard deviation of a turbulent parameter and its turbulent flux is nearly constant or function, e.g. of stability. These so called integral turbulence characteristics are basic similarity characteristics of the atmospheric turbulence (Kaimal and Finnigan 1994; Foken and Wichura 1996).These functions depend on stability and have the general form for standard deviation of wind components. (Foken and Mauder, 2011)

Tab. 5 Overall flag system after Foken (1999), deviations in %

Steady state (flag)	Integral turbulence characteristic (flag)	Steady state (deviation in %)	Integral turbulence characteristic (flag)	Final flag
1	1-2	0-15	0-30	1
2	1-2	16-30	0-30	2
1-2	3-4	0-30	31-75	3
3-4	1-2	31-75	0-30	4
1-4	3-5	0-75	31-100	5
5	≤5	76-100	0-100	6
≤6	≤6	0-250	0-250	7
≤8	≤8	0-1000	0-1000	8
9	9	>1000	>1000	9

The classification 1-3 refers to high quality data, which can be used in the study. 4-6 present moderate quality data, they are only suitable in long term studies. The data, which are classified in 7-9, should be filtered out. To fill these gaps in the data series a gap filling program is necessary.

4.5 Gap filling

The obtained data sets contain gaps due to bad data qualities caused by unsuitable meteorological conditions, malfunction of instruments or other causes. A gap filling process will fill these absent data so that the net ecosystem exchange of those fluxes can be calculated.

4.5.1 Background of gap filling method

There are three main problems by the measurement using the eddy covariance method.

1. As mentioned, gaps due to unfavorable micro-meteorological conditions and instrument failure are inherent in the data stream. Thus a standardized filling of those gaps is necessary (gap-filling), e.g. to obtain daily, monthly or annually integrated balances.

2. The eddy covariance method measures the net ecosystem exchange. However, particularly for the CO_2 exchange, a lot more understanding about ecosystem processes is gained when the net flux is partitioned into its main components, i.e. the gross carbon uptake (GPP) and the ecosystem respiration (Reco).

3. During stable stratification and low turbulent mixing, the eddy covariance method faces several problems that introduce bias and uncertainties. These problems primarily happen during night and lead to an underestimation of the night-time flux, i.e. the ecosystem respiration. These problems can be detected via a micrometeorological quality control that tests if the assumptions of the eddy covariance method are not too strongly violated for a particular half hour. (e.g. Foken & Wichura, 1996). Under circumstances where the necessary information for those tests is not available, a heuristic class of methods is widely accepted that assumes that a threshold of friction velocity (u*) can be site and season specifically established above that night-time fluxes are considered valid. This threshold is usually established by relating the night-time flux to friction velocity while accounting for temperature as a covariate (u*-filtering). (Eddy covariance gap-filling & flux-partitioning tool, Max Planck Institute for Biogeochemistry)

4.5.2 Gap filling method

The gap-filling of the eddy covariance and meteorological data were performed through methods that are similar to those presented by Falge *et al.* (2001), but that consider both the co-variation of fluxes with meteorological variables and the temporal auto-correlation of the fluxes (Reichstein *et al.* 2005).

Due to the missing flux data, the relevant meteorological data was also meanwhile partly missing. The reference station in Hüffergarten, however, offers contemporaneous meteorological data, so that only the data of fluxes are missing, but meteorological data are available (case 1, see 'Background' in the section 'Gap filling' above). In this case, the missing value is replaced by the average value under similar meteorological conditions within a time-window of 7 days. Similar meteorological conditions are present when Rg, Tair and VPD do not deviate by more than 50 W m^{-2}, 2.5 °C, and 5.0 hPa, respectively. If no similar meteorological conditions are present within the time window, the averaging window is increased by 14 days. In case 2, air temperature or VPD data is missing, but radiation is available, in case 3 radiation data is missing as well. The second and third cases, which may be caused by the technical problems at the reference weather station, account only a small part.

Tab. 6 Quality classification scheme for gap-filled values, according to method used and averaging time window.

Averaging-time window	Method		
(in days)	1	2	3
0.5	n.a	n.a	A
1.5-2.5	n.a	n.a	B
>2.5	n.a	n.a	C
7	A	A	n.a
14	A	B	n.a
>28	B	C	n.a
>56	C	C	n.a

A: best; B: acceptable; C: dubious. The classification is based on the notion, that the estimation of the missing data improves with the knowledge on meteorological conditions and with the use of the temporal auto-correlation of the variable that favors smaller time-windows.

(Eddy covariance gap-filling & flux-partitioning tool, Max Planck Institute for Biogeochemistry)

5 Results

5.1 Half-hourly means of CO_2 flux

Half-hourly means of CO_2 fluxes are presented through boxplots in Fig.6. It is obvious that the CO_2 flux was larger in winters than in the other three seasons. Meanwhile, it is also worth to notice that the winter of 2011 had a tremendously large CO_2 flux in comparison to the winter of 2012. The average air temperature showed that 2011 had a colder winter than 2012, especially in February.
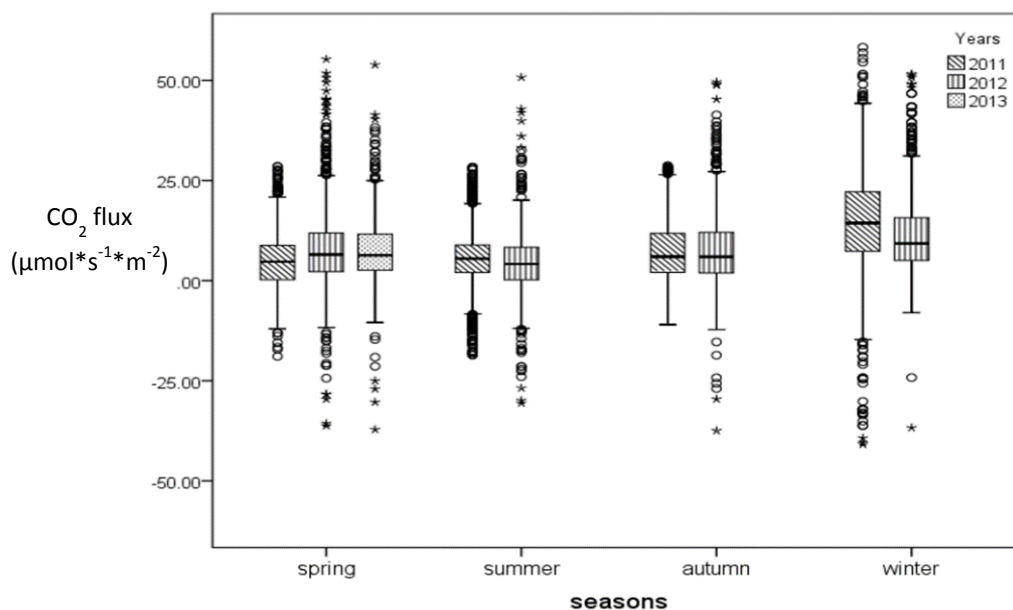
Fig. 6 Half-hourly means of the CO_2 flux, divided into 4 seasons from April 2011 to May 2013.

The bottom and top of the boxes represent the first and third quartiles in the data series, respectively. The lines inside the boxes refer to the medians. Outliers were plotted as individual points with dots, small circles, or stars. Dataset of CO_2 flux was filtered according to Foken.
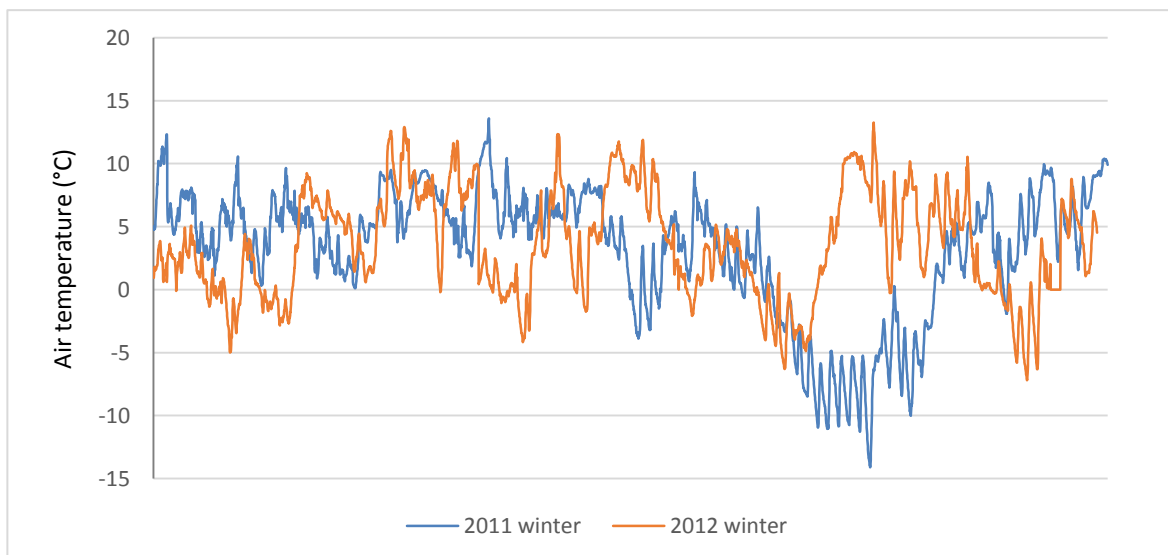
Fig. 7 Half-hourly means of air temperature in 2 winters. (Average value in 2011: 3.18 °C and in 2012: 3.56 °C).

5.2 Average diurnal variation of CO_2 flux

Figure 8 presents the average diurnal course of the CO_2 flux. The maximum value emerged at 8:30 hrs. The flux increased dramatically after sunrise, reaching the peak of 13.15 µmol m^{-2}s^{-1}, then slightly decreased till 12 hrs and kept at a steady level between 7.02 µmols^{-1} m^{-2} and 8.18 µmol m^{-2}s^{-1}. After 17:30 hrs, the CO_2 flux increased again, fluctuating at a range between 8-10 µmol $^{-2}$s^{-1}. After 21:30, however, it decreased continually and the lowest flux occurred at 2:30 hrs at night with a value of 4.52 µmol m^{-2}s^{-1}. To figure out the effects of the classification of the quality control on the diurnal CO_2 courses, the dataset, which included the 7th class were also represented below. There was not apparent difference, except the maximum value showed half of an hour sooner. The data from the 7th class in Foken system would been seen as confidential and also input in the gap filling program as original data.
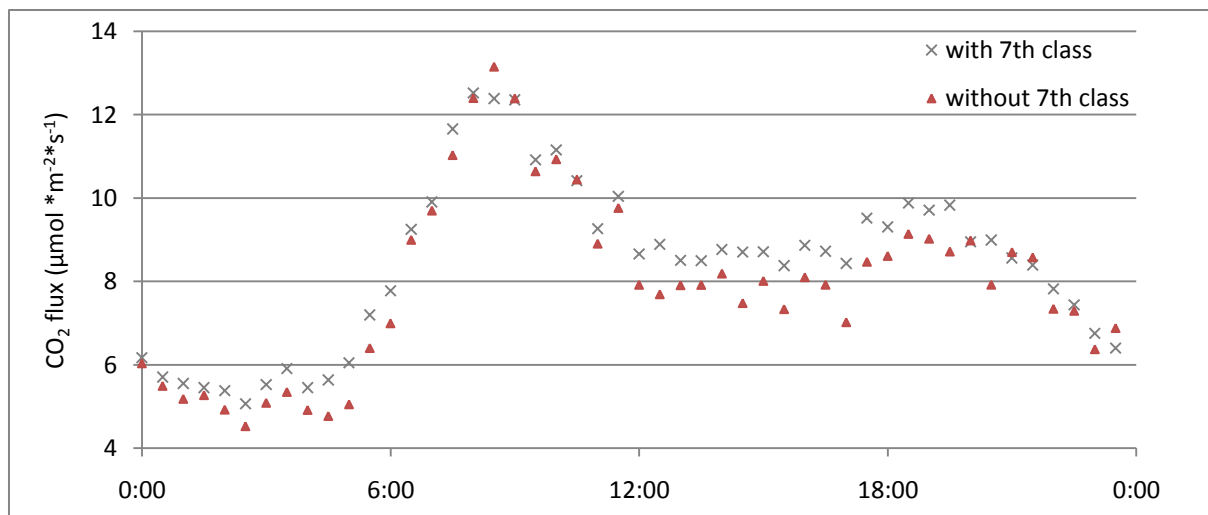
Fig. 8 Average diurnal CO$_2$ flux with an interval of 30 minutes (dataset were calculated after de-spiking and quality control, blue crisscross pattern refers to the dataset, which included the 7th class by the quality controlling; red triangle refers to the dataset, which do not include the 7th class.)

5.3 Correlation between diurnal CO$_2$ flux and air temperature in springs

Figure 9 and table 7 below depict the diurnal CO$_2$ flux and air temperatures during the three different spring periods. In Comparison to 2012 and 2013, the spring of 2011 had higher average temperatures but, at the same time, a less pronounced CO$_2$ flux. In the afternoon, the flux direction inverted and a weak CO$_2$ deposition of -1 µmol m^{-2} s^{-1} was observed. Maxima of air temperatures emerged in the afternoon with 21.6 °C at 16:30 in 2011, 16.9 °C at 17:30 in 2012 and 14.7 °C at 18:30 in 2013. Minima appeared in the mornings, differing at 6:30, 7:30 and 8:30, with 11.7 °C, 11.6 °C and 9.6 °C for 2011, 2012, and 2013, respectively.

Maxima of CO$_2$ fluxes were recorded at 8:00 hrs, whereas minima occurred at different times of the day. The fluxes in three springs apparently did not have the same differences after sunset as after sunrise. Additionally, the greatest variation aroused between 8:00 to 20:00. Although the CO$_2$ flux fluctuated among the 3 springs, they had a similar diurnal pattern as shown in Figure 8.

Tab. 7 Maxima and minima values of CO$_2$ fluxes and air temperatures and their related times

Years	CO$_2$ flux (µmol/s/m^2)				Air temperature (°C)			
	Max.	Time	Min.	Time	Max.	Time	Min.	Time
2011	10.42		-0.78	**14:30**	21.64	16:30	11.74	6:30
2012	14.01	8:00	3.70	3:00	16.98	17:30	11.62	7:30
2013	14.24		1.10	2:00	14.75	18:30	9.64	8:30
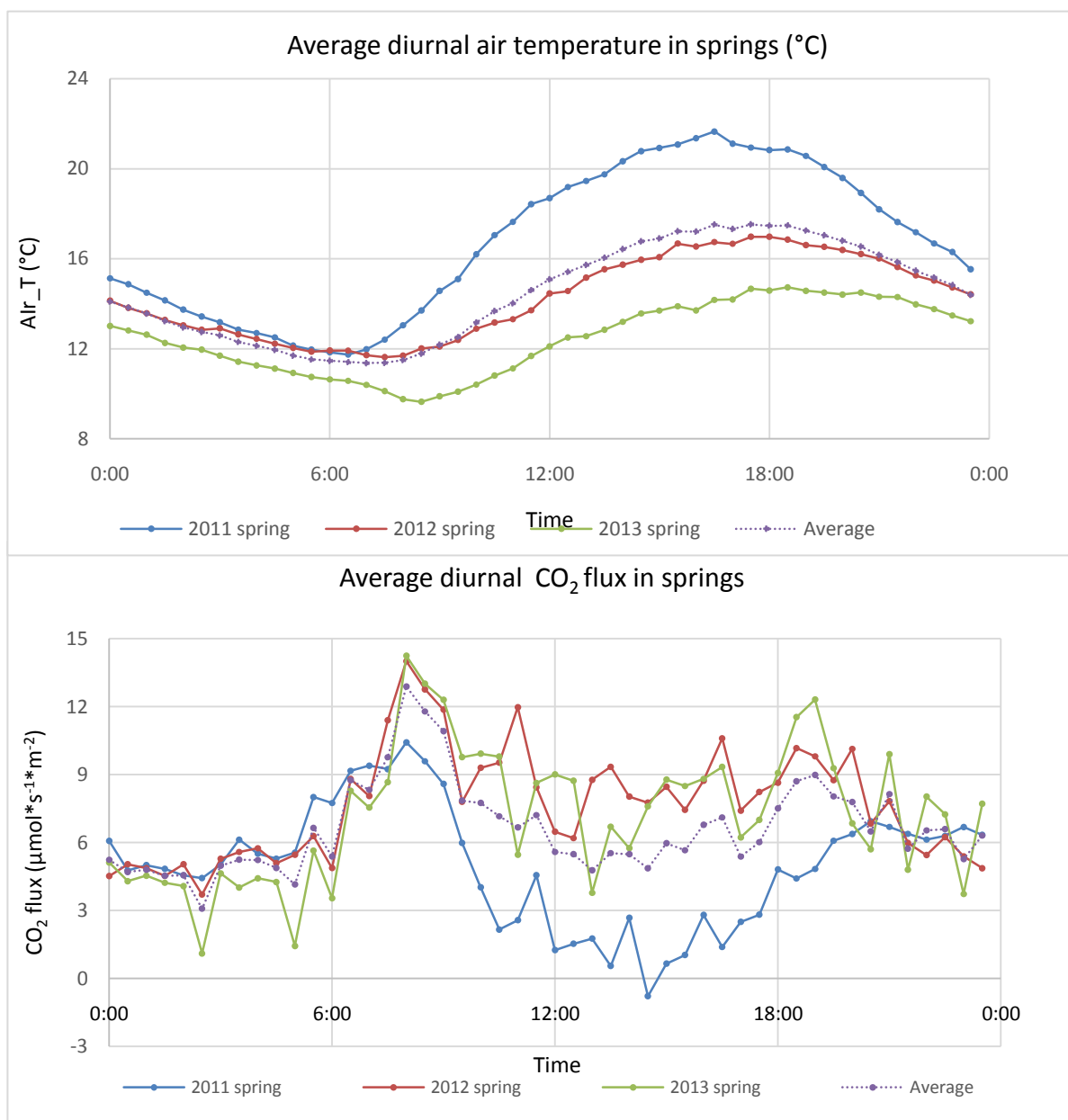
Fig. 9 Average diurnal air temperature in springs and average diurnal CO$_2$ flux in springs (Data of air temperature were collected from the radio tower; data were calculated after de-spiking and quality control)

5.4 Correlation between sensible heat flux and short-wave radiation

In order to analyze the correlation between sensible heat flux and short-wave radiation, the incoming short-wave radiation data from the Hüffergarten site and from the study period (7th April 2011 – 22nd May 2013) are plotted in the bar graph below (Fig. 10). Sensible heat flux, which were measured at the radio tower at the same period, were plotted in the boxplot (Fig.11).
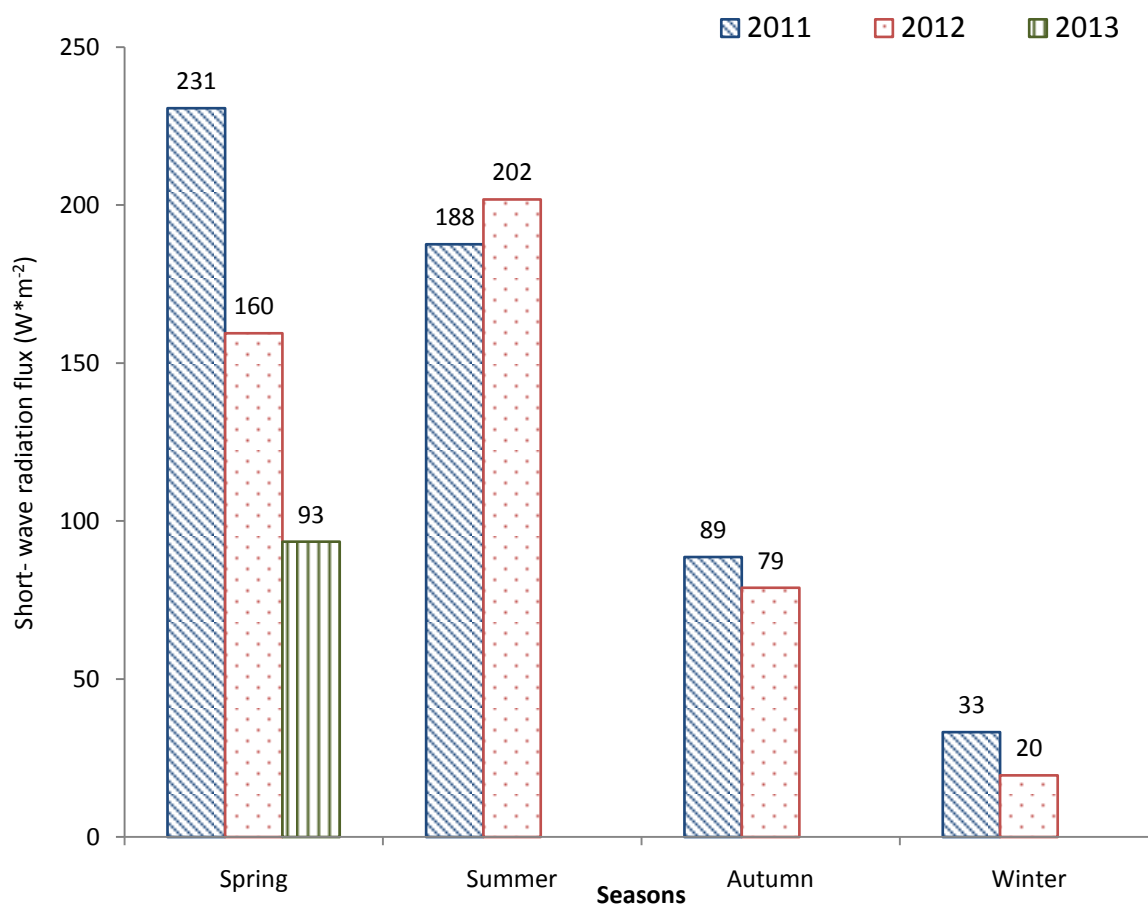
Fig. 10 Seasonal half-hourly means of short-wave radiation (W/m^2) (radiation data were from Hüffergarten)
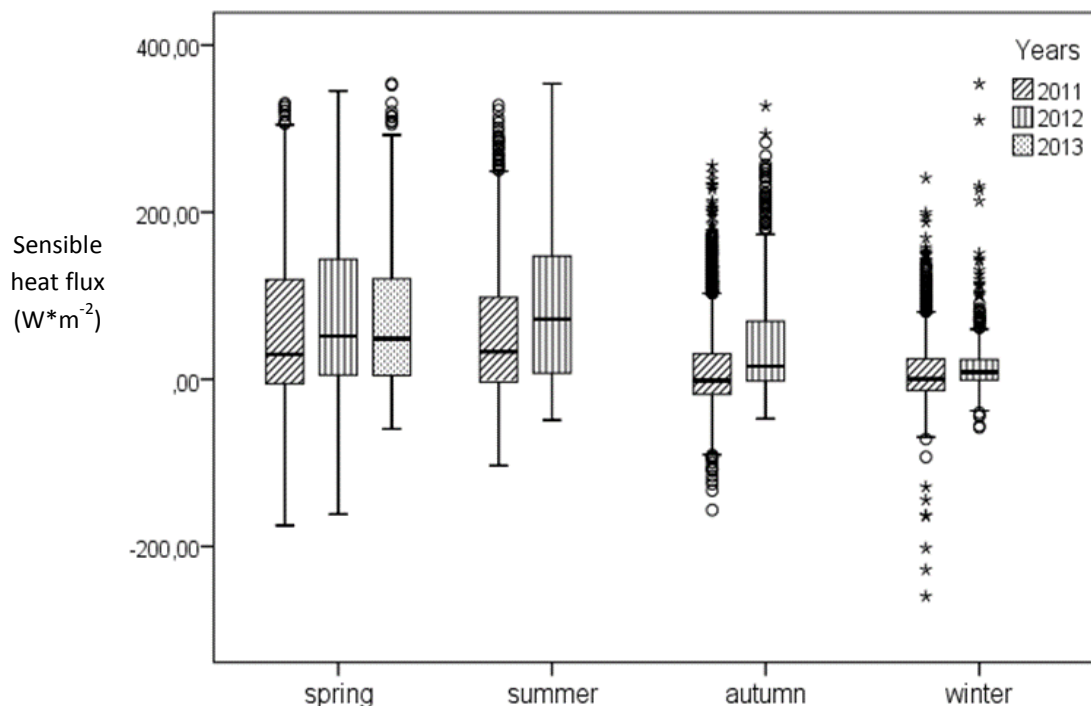
Fig.11 Seasonal half-hourly means of sensible heat (W m⁻²), data were calculated after de-spiking and quality control

It is known that sensible heat flux is the most pronounced in spring and summer due to stronger solar radiation than in autumn and winter (Grimmond and Oke, 1995). In the spring of 2011, the short-wave radiation was even larger than in summer. Compared with other springs, the radiation was much weaker in the spring of 2013, only 40.2 % of the radiation in the spring 2011 and 58.1 % of the radiation in the spring 2012. Furthermore, seasonal sensible heat fluxes had similar features as the short-wave radiation. For example, sensible heat fluxes showed a lower value in summer than in spring in 2011. Although the air temperature was particularly higher in the spring of 2011, the sensible heat fluxes did not have a remarkable value, because the sensible heat flux is related more closely to the short-wave radiation.

5.5 Seasonal variation of water vapor flux and its correlation with CO_2 flux and air temperature

Since the latent heat is important with reference to the phase transition of the water between the surface and the atmosphere, the water vapor flux can represent the latent heat flux. Therefore, only the vertical flux of water vapor is plotted in Figure 12.

A decreased water vapor flux can be observed with increasing temperatures from summer to winter.
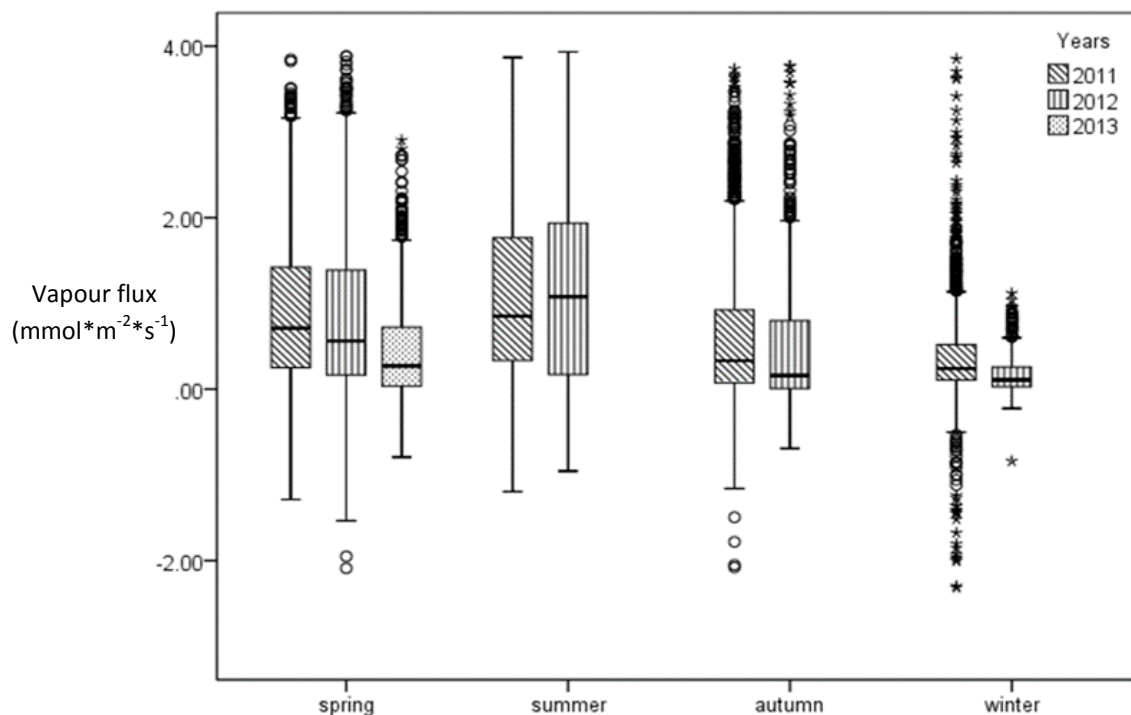
Fig. 12 Seasonal half-hourly means of water vapor flux (mmol m^{-2} s^{-1}), data were calculated after de-spiking and quality control

Viewing the diurnal variation of vertical fluxes of CO_2, water flux and air temperature, they all had a relative low value from 0:00 to 6.00. The water vapor flux had an overall similar tendency like the air temperature, but it altered more strongly. From 6:00 to 8:30, vertical fluxes of CO_2 and water vapor increased rapidly. Afterwards, water vapor flux continued to rise and in contrast to that CO_2 flux began decrease. CO_2 flux increased slightly after 17:00. On the contrary, H_2O started to decrease strongly. Both the CO_2 and H_2O flux had smaller values at night. In total, during the day (8:30-18:30), the CO_2 flux had a negative correlation with water vapor ($R^2 = 0.83$)
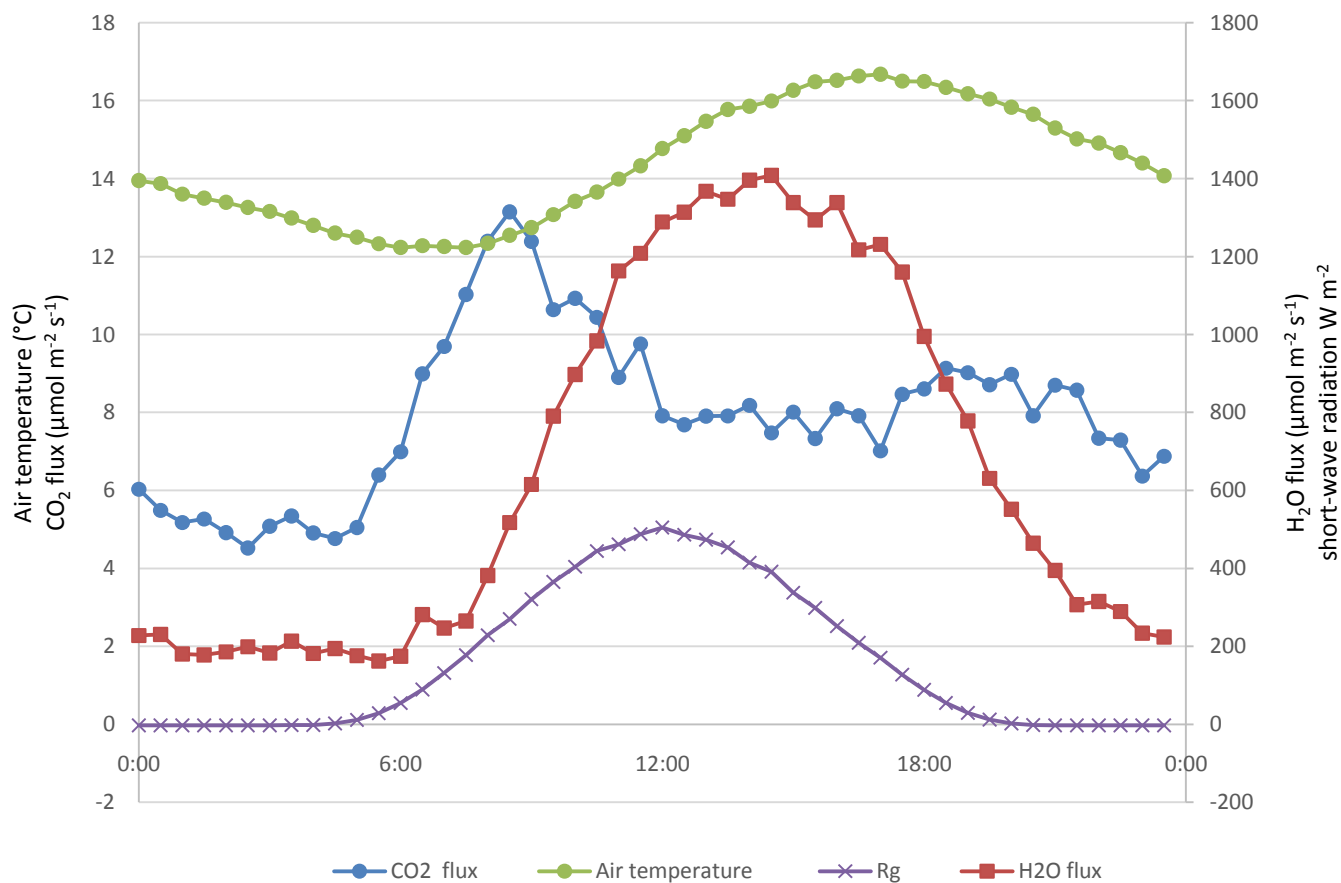
Fig. 13 Courses of average diurnal CO_2-, vapor flux, air temperature and short-wave radiation (calculation of CO_2-, vapor flux after de-spiking and quality control)

5.6 Gap filling

One of the main purposes of this study was to calculate the annual net ecosystem exchange (NEE), which can be calculated through carbon dioxide flux. Because NEE is usually supplied by a unit of C kg m^{-2}a^{-1}, the data gaps of the carbon dioxide flux must be filled. For this purpose, a gap filling tool provided by Max Plank Institute of University of Jena, Germany, using the algorithm described by Reichenstein et al. (2005) was used.

Experimental raw data in 2011 had a completeness of 76.3 %. After filtering of spikes, measurement errors, large AGC values (> 70) and bad quality according to Fokens 1-9 scheme (> 6), 68.5 % of the raw data was still available, the completeness dropped to 52.2 %. Accordingly, 47.7 % of the data had to be filled in by a gap-filling procedure. Compared to 2011, experimental raw data in 2012 had a higher temporal constancy, which was 80.2 %. However, after filtering of spikes, measurement error, large AGC values (> 70) and bad quality (> 6), only 35.3 % of the raw data remained; the temporal constancy fell to 29.8 %. Thus, the data, which in the 7th level classified by the quality control were additionally used in the gap, fill so that the completeness reached 70 %. According to the classification within the gap filling method, 96.4 % of the filled data belonged to the best class in 2011; the acceptable class account for 3.6 %, and 0.01 % was classified as dubious. In 2012, the best class made up 90.6 %, acceptable accounted for 8.16 %, and 1.12 % was classified as dubious.
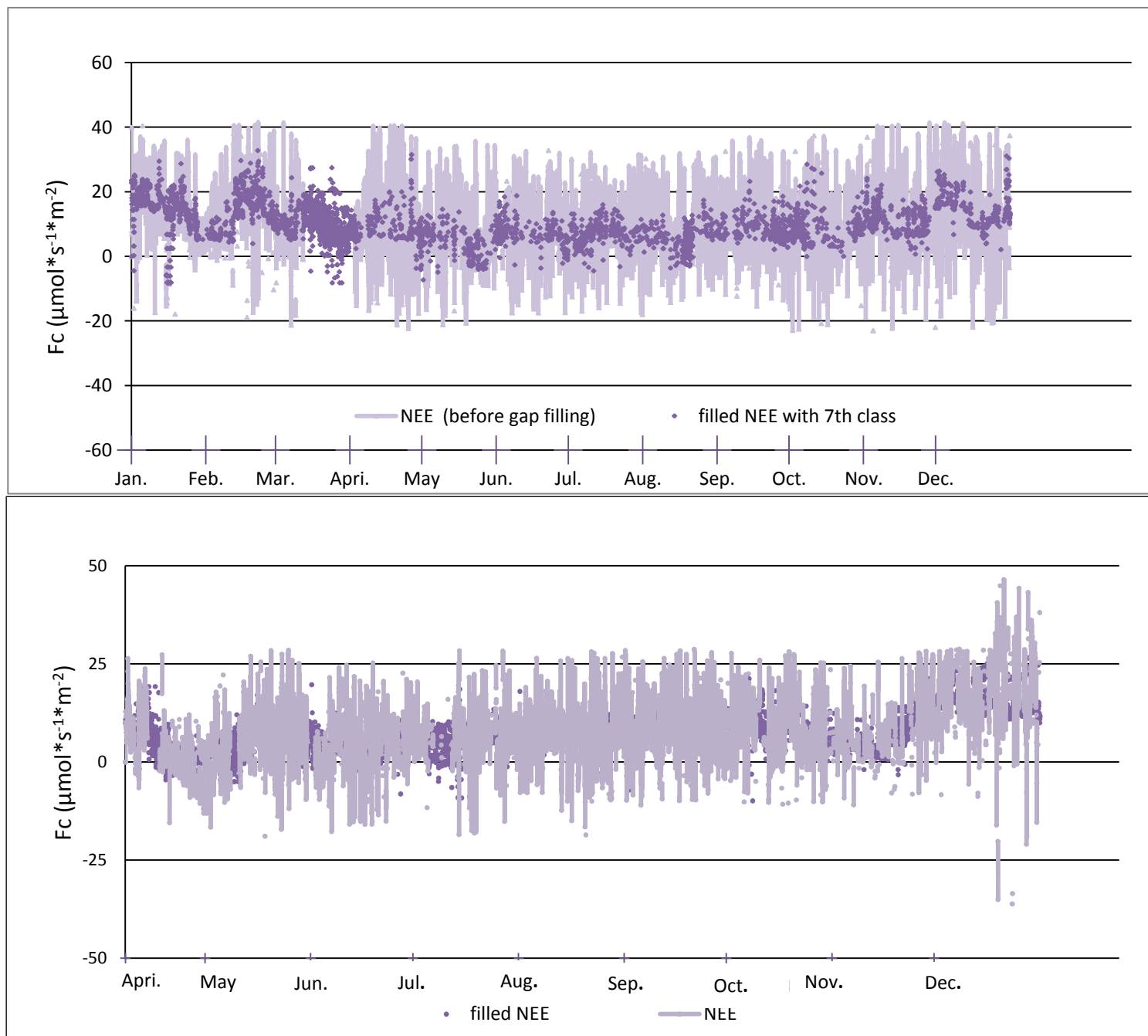
Fig. 14 (top panel) Gap Filling Process for NEE from April to December 2011; (bottom panel) Gap Filling Process for NEE (included 7th class) from January to December in 2012; original experimental data are shown in bright purple and filled gaps are figured with dark dots.

The online Gap filling tool provided the illustrations with color gradients for CO_2 flux before and after gap filling. The gaps within the original data series were filled with averaged values from the existing data base that had been collected during similar meteorological conditions, and temporally as close to the data gap as possible. The sizes of the selected time windows determine the gap filling quality. For example, if the CO_2 flux data was filled with an average values

from within a time window of 7 - 14 days, the filled gaps were classified as confidential (Reichenstein et al., 2004). Since the continuous meteorological data set from the Hüffergarten was used as supplement for the missing ones at the tower, we only have gaps in flux data set. But not in the meteorological data set. Although most of gaps were filled within the best category A, there still were some gaps in the data series, because no similar meteorological conditions were present within the time window of 7 - 14 days. Thus, the averaging window was increased by 28, 56 or more than 56 days in category C, by then, the filled data could have a dubious quality due to the larger time window.

There was a similar character in all of the three graphs in Fig. 15. Negative CO_2 fluxes emerged in spring and summer, the lowest points were even spotted in the afternoon in May because of an extremely warm spring in 2011. Positive fluxes were much more pronounced than the negative ones, Maxima (noted in red to orange) were detected during the whole day in winter but only in the morning hours during the other seasons.
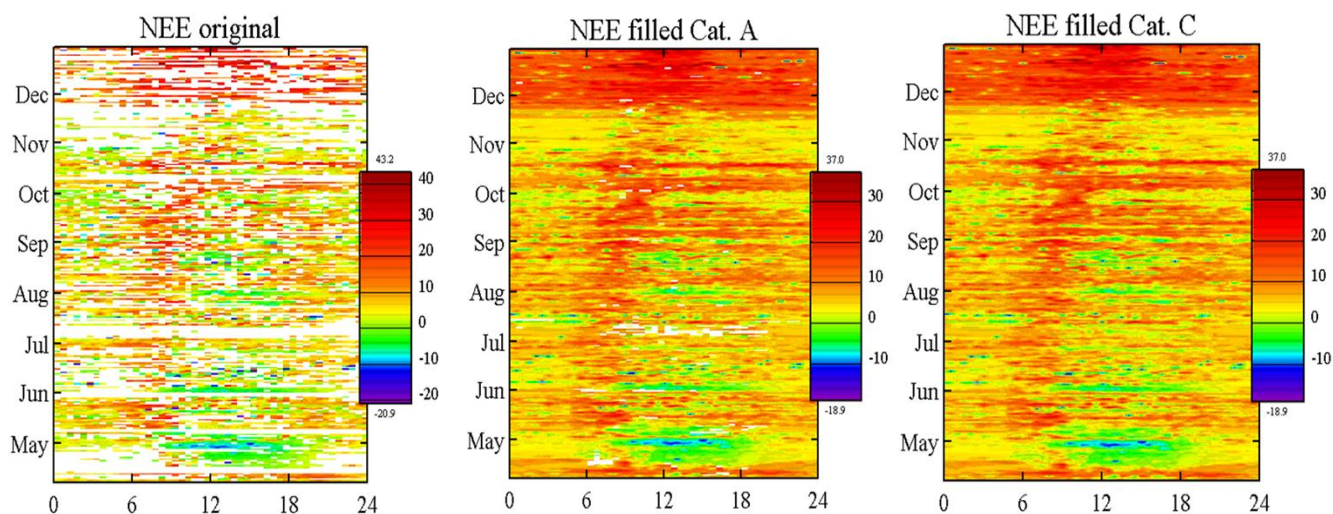
Fig. 15 Original and filled data of CO_2 flux (μmol*s^{-1}*m^{-2}) in 2011 (From left to right: Original CO_2 flux, filled CO_2 flux in category A, filled CO_2 flux in category C, x-axis refers to 24 hours on the day and y-axis represents the seasons)

5.7 CO_2 flux distribution along the wind directions measured at the radio tower

As discussed in Chapter 'Measurement sites description', the measurement at the radio tower captured the urban footprint well, so that most CO_2 fluxes of the whole city would be recorded. However, their strengths depended on the exact urban structures. In Fig. 16, the magnitude of CO_2 fluxes are compared to

the wind directions. The plot reveals that maximum CO_2 fluxes originate from two sectors: 0-45° and 180°- 360° (over West), respectively.
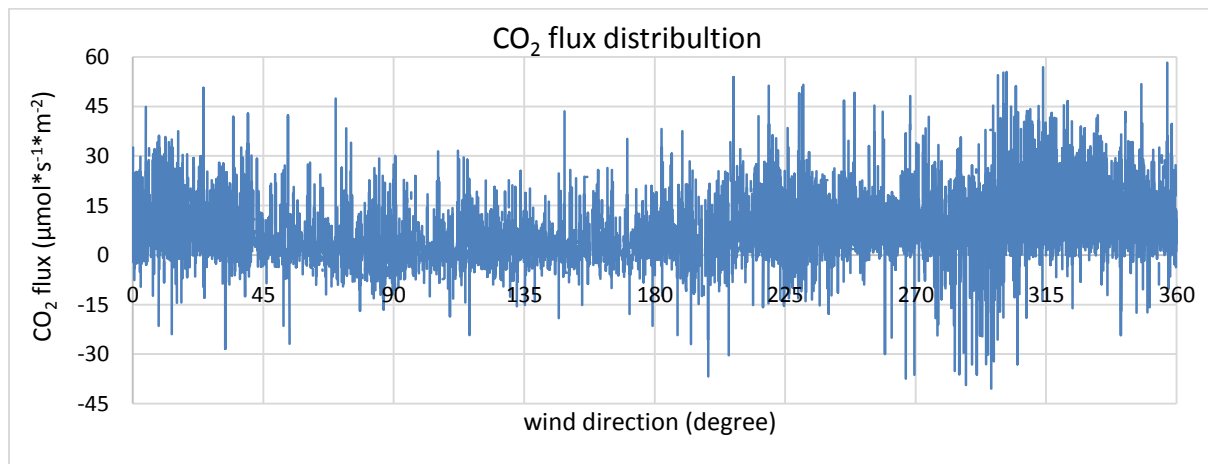
Fig. 16 Distribution of CO_2 flux along the wind direction

5.8 Net ecosystem exchange in 2012

After gap filling process, the missing carbon dioxide fluxes in the original data series were filled. In other words, for each 30-minute there was an average value of carbon dioxide flux. Through summing the 30-minute average values and converting the units the annual net ecosystem exchange can be calculated. In 2012, NEE accounted for 3.26 kg C m^{-2} (without using the 7th class data) and 3.56 kg C m^{-2} (using the 7th class data).

6 Discussion

6.1 Diurnal variation in CO_2 flux

Viewing the average diurnal variation of CO_2 (Fig. 8), the flux increases after the sunrise at 6 hrs because of the increasing traffic and the establishment of atmospheric boundary layer and reaches the maximum at 8:30 when the morning traffic peak appears. Afterwards, photosynthetic activities drive the CO_2 flux slowly down and let it stay at a lower level in the afternoon. Since the CO_2 used in the photosynthesis can only partly counteract the emission in the urban area, the value is still positive. From 17:30 to 20:00, the afternoon traffic peak appears and during this time CO_2 flux increases slightly. At the end of the day, it drops back to a low level due to the absent sunlight and establishment of the stable layer at the night.

6.2 Seasonal fluctuation in CO_2 flux

The photosynthetic activities of plants cause the seasonal fluctuation of CO_2 flux. Plants begin to photosynthesize in the growing seasons like spring and summer; in the photosynthesis process carbon dioxide is consumed and synthesized as chemical energy like sugar. This brings a decrease in CO_2 concentration from March to August. Once winter comes, deciduous plants lose most leaves and the vegetation has a much weaker photosynthesis. On the other hand, respiration by plants, which is photosynthesis in reverse, takes place constantly. Respiration consumes oxygen and sugar and releases carbon dioxide instead. During the day, the CO_2 uptake through photosynthesis outweighs CO_2 emissions through respiration. However, due to anthropogenic emission sources like traffic, fossil fuel combustion and domestic heating in the cold season, the carbon dioxide fluxes are likely to still be positive. Air temperature in the winter plays a role in the CO_2 concentration, as colder winters bring a higher frequency of uses of heating or burning of fossil fuels, which results in more CO_2 emission into the urban boundary layer (apparent in Fig.6, half-hourly means of the CO_2 flux as divided into 4 seasons from April 2011 to May 2013; Fig7, half-hourly means of air temperature in 2 winters). In contrast, during the growing seasons it is also possible to observe a negative CO_2 flux, if the air temperature is outstandingly high. In the afternoon during spring, the photosynthesis can be extremely active so that the emission of CO_2 could be balanced or even outweighed. The air temperature in spring 2011 differed obviously from the other two spring seasons, especially during the days. Hence, the CO_2 flux during this time was lower because of the high

temperatures (Fig. 9). In conclusion, the CO_2 flux has a negative correlation with the air temperature during the days in spring.

6.3. Correlation between sensible heat flux and short-wave radiation

When incoming short-wave solar radiation, known as insolation, enters the Earth's climate system, part of it is absorbed from the Earth's surface, causing the surface to heat up (Wallace and Hobbs, 1977). The intensity of incident shortwave solar radiation at the surface of the earth is dependent on atmospheric absorption and scattering, cloud cover and particulate reflection (Oke TR. Boundary layer climates. 2nd ed. London: Routledge; 1987). Figure 10 and 11 show the positive correlation between sensible heat flux and short-wave radiation. Due to the longer daytime and stronger solar radiation, sensible heat flux was obviously larger in spring and summer. It is possible that short-wave radiation in spring is stronger than in summer, if it has more sunshine hours than summer. According to the meteorological records in Münster, in spring of 2011, sunshine hours totaled up to 688.4 hours, however, in summer only to 474.5 hours (WetterKontor.de). That explained why the spring 2011 has a stronger radiation than the summer, also more sensible heat.

6.4 Seasonal variation of water vapor flux and its correlation with CO_2 flux and air temperature

The CO_2 flux should have a negative correlation with the air temperature through the photosynthesis by plants. Oppositely, the water vapor flux should have a positive correlation with the air temperature through transpiration and evaporation. However, since the study was conducted in an urban area, anthropogenic activities influence the fluxes strongly as well. As shown in Fig. 8, the CO_2 flux had two peaks during the day due to the active traffic in the morning and in the later afternoon. During that time, the CO_2 flux did not show the usual behavior, only after 8 before 18, it built a negative correlation with the air temperature and water vapor flux. A study in Łódź center in Poland showed a great difference in CO_2 flux between urban and rural areas.

The measurements of CO_2 flux conducted in central Poland during cold season 2011-12, as it was expected, show large differences in intensity of carbon dioxide exchange between urban and agricultural surfaces and the atmosphere. During the same period of time, within the Łódź centre mean turbulent net exchange of CO_2 was positive during day and night and many times more intensive. (Pawlak et al. 2012)
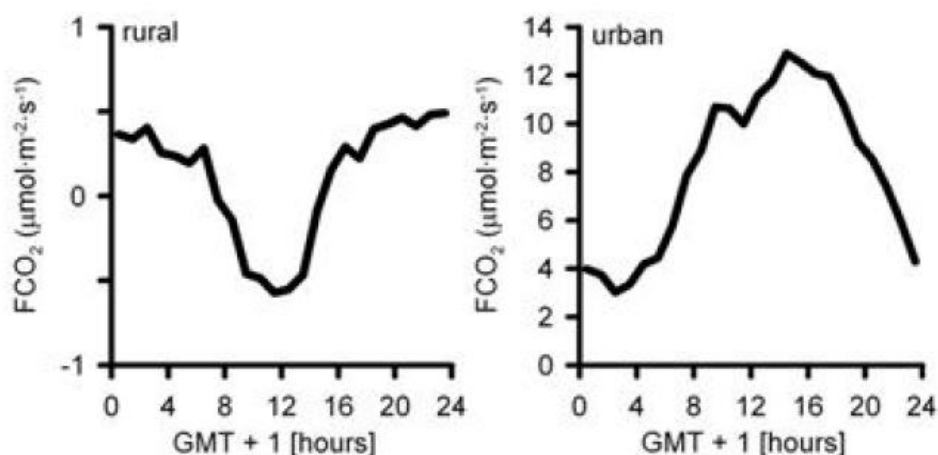
Fig. 17 Mean diurnal courses of carbon dioxide flux in the period November 2011 - April 2012 at urban (Łódź centre) and rural (Annosław) areas (Pawlak et al. 2012)

6.5 Influences of urban structure on the strength of carbon dioxide flux

Since the radio tower is located at the south-eastern section of the city and additionally, south-westerly and westerly wind directions dominate, most of the emissions from the city can be captured at the tower. As discussed in the 'Result' section 7, the stronger carbon dioxide fluxes emerged in the sectors of 0-45 degree and West (180-360 degree). It can be observed in the map below (Fig. 19) that the western section includes the settlements, the railway station, harbor and its relevant industrial territories, three main streets (Warendorfer Str., Wolbecker Str., and Hohenzollernring) and the whole city center. In contrast, another section (45°-180°) has more green areas. In summary, it can be said that the anthropogenic activities like vehicles, residential districts, influence the emission strongly.
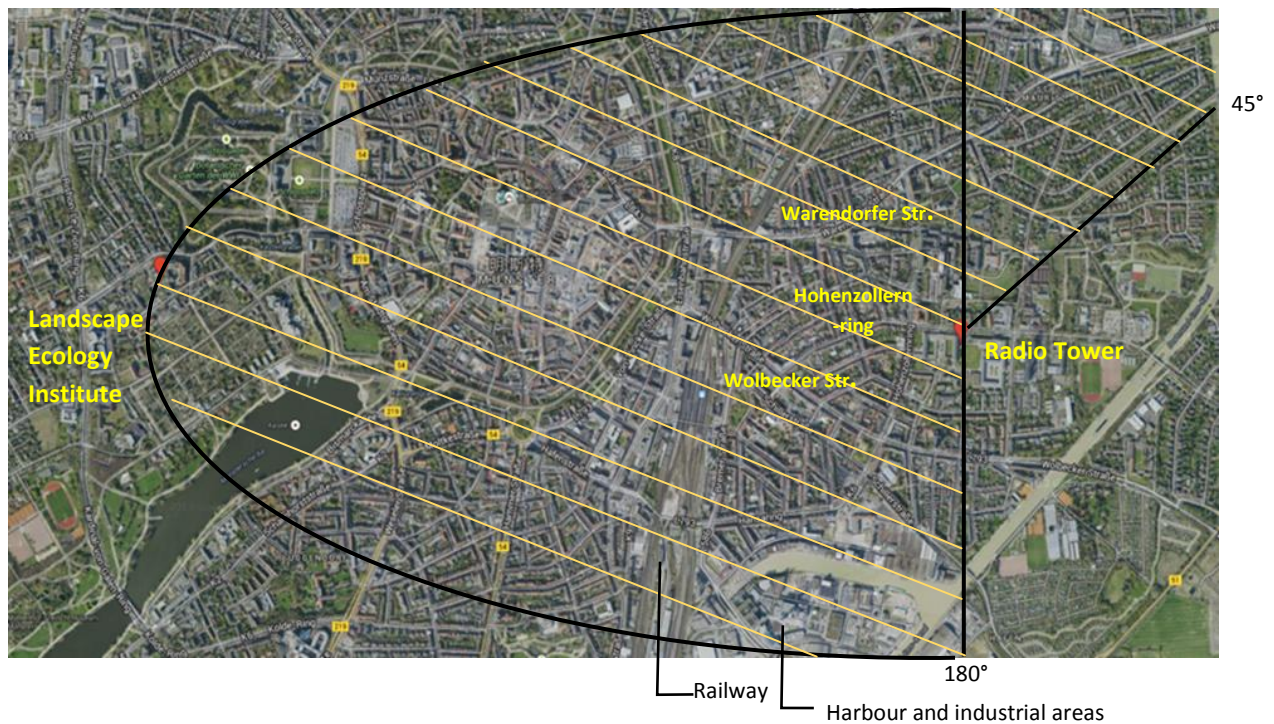
Fig. 18 Description of urban distribution and stronger CO$_2$ fluxes (areas with yellow lines)

6.6 Urban net ecosystem exchange

With the software 'Eddy Pro', the quality of fluxes were examined and categorized in 9 classes according to Foken system. In 2012, only 35.5 % of the raw data remained for the gap filling program because in the dataset approximately one half of the data was classified into the 7th category. To improve the accuracy of the gap filling process, the quality 7 part of the dataset was also used in a second gap fill run so that only 30 % of the raw data was missing. This resulted in a NEE value of 3.56 kg C m^{-2}a^{-1}, which is slightly higher (9 %) as compared to the original one (3.26 kg C m^{-2} a^{-1}).

In a city, which is intensively influenced through humans, the most significant source of CO$_2$ is anthropogenic emission related to mineral fuel combustion, car traffic or heating by the energy industry, which is observed particularly during the cold season (Grimmond et al., 2002; Nemitz et al., 2002; Moriwaki and Kanda, 2004; Gratani and Varone, 2005; Coutts et al., 2007; Vesala et al., 2008; Roth and Velasco, 2010). Only during the warm season anthropogenic emissions are mitigated to a certain degree by natural CO$_2$ absorption through photosynthesis (Grimmond et al., 2002; Moriwaki and Kanda, 2004; Vesala et al., 2008). Nevertheless, it still behaves as an apparent source of carbon dioxide emission annually. In this study, Münster city emits 3.26 kg C m^{-2}a^{-1} (2012 as the example year). Recent studies reveal several figures about the urban NEE.

Copenhagen had a NEE value with 3.49 kg C $m^{-2} a^{-1}$ in 2003 (Soegaard, H., Møller-Jensen, L., 2003). A study in the capital city of China, Beijing gave a NEE of 5.62 kg C $m^{-2} a^{-1}$ in 2007 (Song and Wang, 2011). A suburban site (Preston) in Melbourne, Australia gave out 2.31 kg C $m^{-2} a^{-1}$ in 2004. There is some information about those cities (Tab. 8).

Tab. 8 Area and population of the cities and their related annual NEE

City	Münster	Copenhagen	Beijing	Preston in Melbourne
Area (km²)	302.9	88.25	16801	11.3
Population	291754	559440	11510000	29922
Annual NEE (kg C/m²)	3.26	3.49	5.62	2.32
Year	2012	2003	2007	2004

It can be observed that the metropolis Beijing with higher population had an extreme emission of carbon dioxide compared to the cities with a smaller population like Münster or Copenhagen. In contrast, in the suburban area, Preston in Melbourne, the annual emission is much weaker. According to a study over a boreal scots pine forest (Markkanen et al., 2001); the estimated annual balances of the NEEs were -234 g C m^{-2}, -262 g C m^{-2} and -191 g C m^{-2} in 1997, 1998, and 1999, respectively.

A study in Helsinki in Finland revealed more information about annual carbon balance in other cities, which were measured also at towers (Tab. 9).

Tab. 9 Annual CO$_2$ emissions (NEE, g C m^{-2}) observed in urban studies and the methods used to obtain them. Only studies where more than 12 months have been reported are listed. Also the plan area fractions of vegetation (f$_{veg}$) are given

City	Observation period	NEE (g C m^{-2})	Gap filling method	f$_{veg}$
This study (Helsinki)	Jan 2006-Dec 2010	1760	ANN	0.44
Essen[1]	Sep 2006-Oct 2007	3940	ANN	0.22
London [2]	Oct 2006-May 2008	9690	Daily averages	0.08
Baltimore[3]	Jan 2002-Dec 2006	361	PAR in daytime, Tsoil in night-time	0.67
Vancouver[4]	May 2008-April 2010	6710	Median diurnal cycles	0.34
Montreal-urb[5]	Nov 2007-Oct 2009	5570	From average daily Fc + interpolation	0.29
Montreal-sub[5]	Nov 2007-Oct 2009	1420	From average daily Fc + interpolation	0.5
Tokyo[6]	May 2001- Apr 2002	3350	Look-up tables	0.21
Melbourne[7]	Feb 2004- Jun 2005	2320	GRNN	0.37
Beijing[8]	Jan 2006-Dec 2009	4860	Gap length dependent: interpolation, mean diurnal cycle, multiple imputation method	0.15

[1] Kordowski and Kuttler (2010), [2] Helfter et al. (2010), [3] Crawford et al. (2011), [4] Christen et al. (2011), [5] Bergeron and Strachan (2011),[6] Moriwaki and Kanda (2004), [7] Coutts et al. (2007), [8] Liu et al. (2012)

(Järvi et al., 2012)

The annual carbon emission from Münster is apparently at the middle of this list, which at a similar degree as Tokyo. Additionally, there is 17 % more emission in Essen than in Münster, which makes sense because Essen has higher density of population and influenced by heavy industries in the Ruhrgebiet area.

As mentioned in the published documentation from city halls, Wuppertal, Bonn and Herne had 5.24 kg C m^{-2} (2009), 4.92 kg C m^{-2} (2010) and 5.57 kg C m^{-2} (2010), respectively. The figures were estimated after 'Life-Cycle-Assessment-Faktoren' like household, economy, consumption of energy and traffic, which used a software developed by a Swiss company 'Ecospeed', but the uptake CO$_2$ by vegetation is not taken into account. With the same method, the emissions of CO$_2$ were estimated for Münster to be 2.06 kg C m^{-2} for 2006 (Duscha et al., 2009), 1.91 kg C m^{-2} for 2010, and 1.85 kg C m^{-2} for 2011 (stadt-Münster.de). It is remarkable that these emission estimates are much smaller than the NEE numberds from this study, although they do not include any uptake of CO$_2$ by the urban vegetation. In other words, the measurement from this study are in the order of a factor 2 larger than the emission estimates. The cause for this discrepancy is unclear.

7 Conclusion

The purposes of this study are to present the daily, seasonal and annual carbon dioxide deviation in an urban area through filtering and analyzing the dataset with an eddy covariance system. The results reveal the disctinct carbon dioxide courses in the scales of day, season and year. Additionally, the correlation between CO_2 flux or other energy fluxes and the meteorological parameters is well indicated in the dataset analyzed in this work.

Because of the special character of a city, the CO_2 flux in an urban area also has its features: It is strongly influenced by the human activities, for example, using of heating in the cold seasons, daily traffic peaks in the main streets and industries.

Using the gap filling routine, an annual net ecosystem exchange (3.26 - 3.56 C kg m^{-2}) in Münster was calculated. By comparing with reports from other studies, in which the same method were used, the NEE value from this study made sense. It matched well with the size, the population, landscape types of this city.

List of literatures

Alduchov, O.A., Eskridge, R.E. (1996): *Improved Magnus' form approximation of saturation vapor pressure*. Journal of Applied Meteorology 35:601–609

Buck, A. L. (1981): *New equations for computing vapor pressure and enhancement factor*. Journal of Applied Meteorology 20: 1527–1532

Burba,G. (2013): *Eddy Covariance Method for Scientific, Industrial, Agricultural, and Regulatory Applications.* (Licor.com, published June 2013)

Burba, G., Schmidt, A., Scott, R. L., Nakai, T., Kathilankal, J., Gerardo, F. N. I., Hanson, C., Law, B. E., McDermitt, D. K., Eckles, R., Furtaw, M., and Velgersdyk, M. (2012): *Calculating CO_2 and H_2O eddy covariance fluxes from an enclosed gas analyzer using an instantaneous mixing ratio*. Global Change Biology, 18: 385–399.

Climatemps.com (2009-2014): *Münster Climate and Temperature. http://www.munster.climatemps.com/*

Coutts, A. M., Beringer J., Tapper, N. J. (2007): *Impact of Increasing Urban Density on Local Climate: Spatial and Temporal Variations in the Surface Energy Balance in Melbourne, Australia*. Journal of Applied Meteorology and Climatology 46: 477-493

Deutschland123.de (2013): *http://www.deutschland123.de/muenster*

Deventer, M.J., Griessbaum, F., Klemm, O. (2013): *Size-resolved flux measurement of sub-micrometer particles over an urban area.* Meteorologische Zeitschrift, Volume 22, Number 6, pp. 729-737(9)

Duscha, M., Dünenebeil, F., Gugel, B., Kutzner, F. (2009): *Klimaschutzkonzept 2020 für die Stadt Münster http://www.muenster.de/stadt/umwelt/pdf/klimaschutzkonzept2020.pdf*

Falge, E., Baldocchi, D., Olson, R. et al. (2001): *Gap filling strategies for long term energy flux data sets*. Agricultural and Forest Meteorology 107, 71–77

Fisher, B., Joffre, S., Kukkonen, J., Piringer, M., Rotach, M.W., Schatzmann, M. (2005): *Meteorology Applied to Urban Air Pollution Problems.* Demetra Ltd Publishers, Final report COST Action 715, 276 pp, doi: ISBN 954-9526-30-5

Foken, T. (2003): *Angewandte Meteorologie*. 1 Edition, Berlin

Foken, T., Wichura, B. (1996): *Tools for quality assessment of surface-based flux measurements*. Agricultural and Forest Meteorology, 78, 83-105

Gash, J.H.C., Gulf, A.D. (1996): *Applying a linear detrend to eddy correlation data in real time*. Boundary Layer Meteorology, 79, 301-306

Gietl, J.K., Trischer,T., Klemm, O. (2008): *Size-segregated analysis of PM10 at two sites, urban and rural, in Münster (Germany) using five-stage Berner types impactors*, Atmospheric Environment, Vol. 42, Issue 22, pp. 5721-5727

Gillinstruments.com (2014): *R3-50 Research Anemometer*. *http://www.gillinstruments.com/products/anemometer/R3-50.htm*

Gratani, L., Varone, L. (2005): *Daily and seasonal variation of CO_2 in the city of Rome in relationship with the traffic volume*. Atmospheric Environment 39, 2619-2624

Grimmond, C.S.B., Oke T.R. (1995): *Comparison of heat fluxes from summertime observations in the suburbs of four North American cities.* Journal of Applied Meteorology, 34, 873-889

Grimmond, C.S.B., Offerle, B. et al. (2002): *Observations of local-scale heat, water, momentum and CO_2 fluxes at Cub Hill, Baltimore*. 4th Symp. Urban Environment 10.6

Gurjanov, A.A., Zubkovskii S.L., Fedorov, M.M. (1984): *Mnogoknal'naja avtomatizirovannaja Sistema obrabotki signalov no baze EVM*. Ged. Geophys. Veröff., R, II, 26:17-20

Informatik und Technik Nordrhein-Westfalen AG (2012): *Top Ten der größten Städte. http://www.it.nrw.de/statistik/a/daten/eckdaten/r511dichte.html*

Jamieson, J.A., Mecfee, R.H., Plass, G.N., Grube, R.H., Richards, R.G. (1963): *Infrared Physics and Engineering*. McGrawHill, New York, 673pp.

Järvi, L., Nordbo, A., Junninen, H. et al. (2012): *Seasonal and annual variation of carbon dioxide surface fluxes in Helsinki, Finland, in 2006–2010Intra-city variation in urban morphology and turbulence structure in Helsinki, Finland*. Atmos. Chem. Phys., 12, 8475–8489Boundary-Layer Meteorology, In press

Kaimal, J. C., Finnigan, J. J. (1994): *Atmospheric boundary layer flows—their structure and measurement.* Oxford University press. pp. 289.

Kolle, O., Rebmann, C. (2007): *Documentation of a Software Package to Acquire and Process Eddy Covariance Data.* Max-Plank-Institute for Biogeochemistry, Jena, Germany

Licor.com (2011): *Components of LI-7200 Enclosed CO_2/H_2O Analyzer. http://www.licor.com/env/products/gas_analysis/LI-7200/system_components.html*

Licor.com (2011): *Components of LI‐7500A Open Path CO2/H2O Gas Analyzer http://www.licor.com/env/products/gas_analysis/LI-7500A/system_components.html*

Markkanen, A., Juutilainen, J., Lang, S., Pelkonen, J., Rytömaa, T., Naarala, J. Markkanen A, et al. (2001): *Effects of 50 Hz magnetic field on cell cycle kinetics and the colony forming ability of budding yeast exposed to ultraviolet radiation*. Bioelectromagnetics 22(5):345-50L.

Mauder, M. and Foken, T. (2011): *Documentation and instruction manual of the eddy covariance software package TK3*, Univ. Bayreuth, Abt. Mikrometeorol., ISSN: 1614-89166, 46,58 pp.

Moriwaki, R. and Kanda, M. (2004): *Seasonal and diurnal fluxes of radiation, heat, water vapor and CO2 over a suburban area.* Journal of Applied Meteorology, 43, 1700-1710

Nemitz, E., Gallagher, M.W., Duyzer, J.H., Fowler, D. (2002): *Micrometeorological measurements of particle deposition velocities to moorland vegetation*. Quarterly J Royal Met Soc, 128: 2281-2300

Obukhov, A.M. (1951): *Characteristics of the Micro-structure of the Wind in the Surface Layer of the Atmosphere*. Izv. AN SSSR, ser Geofiz. 3, 49-68

Oke, T.R. (1976): *The distinction between canopy and boundary‐layer urban heat islands.* Atmosphere 14(4), 268-277

Oke, T.R. (1988): *Boundary Layer Climates.* Routledge, 2 Edition

Pawlak, W., Fortuniak, K. and Siedlecki, M. (2011): *Carbon dioxide flux in the centre of Łódź, Poland-analysis of a 2-year eddy covariance measurement data set*. Int. J. Climatol. 31, 232-243.

Reichstein, M., Subke, J.-A., Angeli, A. C., Tenhunen, J. D. (2005): *Does the temperature sensitivity of decomposition of soil organic matter depend upon water content, soil horizon, or incubation time?* Global Change Biology, 11, 1-14

Roth, M., Velasco, E. (2010): Cities as net sources of CO_2: Review of atmospheric CO_2 exchange in urban environments measured by eddy covariance technique. Geography Compass, 4: p. 1238-1259

Schmidt, A., Wrzesinsky, T. and Klemm, O. (2008): *Gap Filling and Quality Assessment of CO_2 and water Vapour fluxes above an Urban Area with RTadial Basis Function Neural Networks*, Boundary Layer Meteorology Vol.126, No. 3. Pp 389-413.

Soegaard, H., Moller-Jensen, L. (2003): *Towards a spatial CO2 budget of a metropolitan region based on textural image classification and flux measurements*. Remote Sensing of Environment 87: 283-294.

Song, T., Wang, Y. S. (2012): *Carbon dioxide fluxes from an urban area in Beijing. Atmospheric Research*. 106: 139-149

Stadt-Münster.de (2013): *Energie- und Klimabilanz der Stadt Münster: Bilanzierung des Energieeinsatzes und der Treibhausgas-Emissionen für die Jahre 1990 – 2011*. Anlage 2 zu V/0293/2013

Swinbank, W.C. (1951): *The measurement of vertical transfer of heat and water vapor by eddies in the lower atmosphere*. Journal of Meteorology. 8:135-145

Vesala, T., Järvi, L., Launiainen, S. Sogachev, A., Rannik, Ü., et al. (2008): *Surface-atmosphere interactions over complex urban terrain in Helsinki, Finland*. Tellus Series B Chemical And Physical Meteorology, 60, 188-199

Wekipedia.com: *Virtual Temperature http://en.wikipedia.org/wiki/Virtual_temperature*

WetterKontor.de: *Monats- und Jahreswerte für Münster / Osnabrück http://www.wetterkontor.de/de/monatswerte-station.asp?id=10315&b=2*

Windfinder.com (2011-2014)*: Wind- & Wetterstatistiken Münster/Osnabrück http://www.windfinder.com/windstatistics/muenster_osnabrueck?fspot=muenster_aasee*

List of figures

List of tables

List of equation

Eidesstattliche Versicherung

Hiermit versichere ich, diese Arbeit selbständig verfasst und keine anderen Hilfsmittel und Quellen als die angegebenen verwendet zu haben.

Münster, August 2014

Yang Zhao